JAAS

Accepted Manuscript

This is an *Accepted Manuscript*, which has been through the Royal Society of Chemistry peer review process and has been accepted for publication.

Accepted Manuscripts are published online shortly after acceptance, before technical editing, formatting and proof reading. Using this free service, authors can make their results available to the community, in citable form, before we publish the edited article. We will replace this *Accepted Manuscript* with the edited and formatted *Advance Article* as soon as it is available.

You can find more information about *Accepted Manuscripts* in the Information for Authors.

ROYAL SOCIETY OF CHEMISTRY

www.rsc.org/jaas

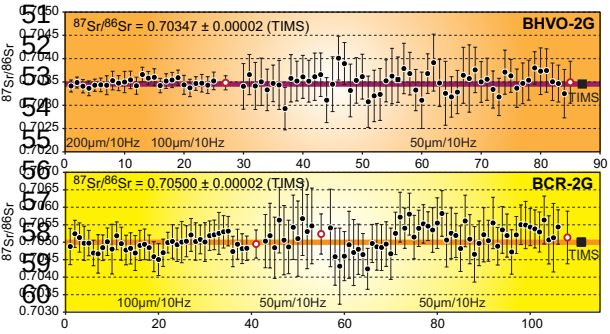

Table of contents entry.
An analytical protocol using LA-MC-ICP-MS for precise Sr isotope ratio analysis from small glass samples is presented.

TECHNICAL NOTE

In situ Sr isotope measurement of small glass samples using multiple-Faraday collector inductively coupled plasma mass spectrometry with 10^{12}-Ω resistor high gain Faraday amplifiers†

Qing Chang*[a], Jun-Ichi Kimura[a], and Bogdan Stefanov Vaglarov[a]

An analytical protocol was developed for correcting Kr baseline-induced bias and Rb isobaric overlap factors to analyse Sr isotope ratios for small glass samples using excimer laser ablation (LA) with an Aridus II desolvating nebuliser dual-intake system and multiple collector inductively coupled plasma mass spectrometry (MC-ICP-MS). Combined use of a low-oxide interface setup, along with high-gain Faraday amplifiers with a 10^{12}-Ω resistor, enabled precise determination of Sr isotope ratios from 50- and 100-µm diameter craters at 10-Hz laser repetition rate. Residual analytical biases of $^{84}Sr/^{86}Sr$ and $^{87}Sr/^{86}Sr$ isotope ratios, obtained from Kr baseline suppressions (Kimura et al., 2013, Journal of Analytical Atomic Spectrometry, 28, 945–957), were found to be nonlinear, but the correction method was applicable to 50–200-µm/10-Hz craters. We also found that the $^{85}Rb/^{87}Rb$ overlap correction factor changed with time with a change in the surface condition of the sampler–skimmer cones. The correction factor of $^{85}Rb/^{87}Rb$ was thus determined at least once per five unknown measurements using the Aridus solution intake line. We determined $^{87}Sr/^{86}Sr$ isotope ratios from MkAn anorthite (Sr = 305 ppm, Rb = 0.07 ppm), BHVO-2G, KL2-G, ML3B-G (Sr = 312–396 ppm, Rb = 5.8–9.2 ppm), and BCR-2G (Sr = 337 ppm, Rb = 48.5 ppm) basalt glasses using a 50–100-µm/10-Hz crater. The results agree well with their reference values, determined by

thermal ionisation mass spectrometry, even with the high Rb/Sr ratio (0.14) in the BCR-2G glass. The internal/intermediate precisions were ±0.0002 (two-standard deviation: 2SD) for 100-µm craters and ±0.0005 for 50-µm craters. The new instrument settings and analytical protocol improved the precision by a factor of two compared to the previous report using LA-(sector field)-ICP-MS and enables the analysis of sample volumes that are ten times smaller than those used in previous LA-MC-ICP-MS analyses with equal precision.

(298 words in abstract, 6836 words in all document)

[a] Department of Solid Earth Geochemistry (DSEG), Japan Agency for Marine-Earth Science and Technology (JAMSTEC), 2–15 Natsushima-Cho, Yokosuka 237-0061, Japan.

E-mail: qchang@jamstec.go.jp; Fax: +81-46-867-9634; Tel: +81-46-867-9765

† Electronic supplementary information (ESI) available: Data Table 1: Analytical results of Sr isotope ratios. See DOI:10.1039/c4jaxxxxxg

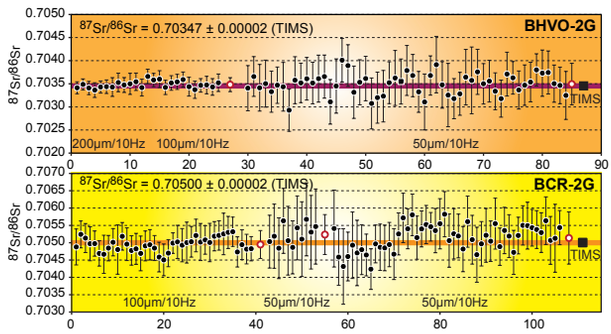

Table of contents entry.
An analytical protocol using LA-MC-ICP-MS for precise Sr isotope ratio analysis from small glass samples is presented.

1. Introduction

1.1.In situ Sr isotope ratio analysis by LA-ICP-MS

Strontium isotope analysis using in situ laser ablation multiple collector inductively coupled plasma mass spectrometry (LA-MC-ICP-MS) has been a useful geochemical tool for the analysis of plagioclase crystals or carbonate materials and glasses.[1-6] Complex isobaric overlaps from Ar gas blanks and isobaric ions, oxides, and doubly charged ions from the samples are of concern for four naturally occurring Sr isotopes, ^{84}Sr, ^{86}Sr, ^{87}Sr, and ^{88}Sr. Data correction protocols are therefore very complex, prompting rigorous examination. These problems and their resulting solutions have been summarized by Vroon et al.[7]

The most commonly employed Sr isotope measurement protocol[7] for the geochemical samples is the use of on-peak background subtraction, which corrects for Kr gas blanks and instrumental memories of Sr and Rb,[1, 2, 5, 6, 8-13] although iterative subtraction of the Kr baselines is also a useful technique.[3, 13] Overlap correction of ^{87}Rb using ^{85}Rb is achieved by an external mass bias correction from Sr, determined as ^{86}Sr/^{88}Sr = 0.1194.[1, 2, 5, 6, 8-12] but is successful only with the actual determination of ^{85}Rb/^{87}Rb, either by measurement of a Rb-doped Sr standard solution, using a solution-laser aerosol-dual intake system,[14] or by measurement of both natural and synthetic glasses with known ^{87}Sr/^{86}Sr isotope ratios.[2, 3, 15] Interferences from Ca dimers, CaAr, and ^{23}Na$^{60–64}$Ni molecular ions are usually negligible for plagioclase crystals and carbonates.[6, 7, 10] Oxide interferences on ^{85}Rb and ^{87}Sr, from ^{69}Ga^{16}O and ^{71}Ga^{16}O are significant for samples rich in Al, such as plagioclase and glass, as Ga has a chemical affinity for Al and is highly partitioned in these samples.[14] Therefore, by using particular MC-ICP-MS settings,[16] high oxide yields are avoided.[6, 10] Interference from doubly

charged rare earth element (REE) ions are also obvious,[10, 12, 17] and care must be taken to exclude REE-rich Sr-poor samples (e.g., clinopyroxene) and co-ablation of REE-rich mineral inclusions (e.g., apatite). The REE double charges such as $^{166}Er^{++}$, $^{168}Er^{++}$, and $^{170}Er^{++}$ for ^{83}Kr, ^{84}Sr, and ^{85}Rb, respectively, and $^{170}Yb^{++}$, $^{172}Yb^{++}$, $^{174}Yb^{++}$ and $^{176}Yb^{++}$ for ^{85}Rb, ^{86}Sr, ^{87}Sr and ^{88}Sr, respectively, can be monitored, or even corrected for, by placing the Faraday collectors at half-mass positions of $^{83.5}M$ ($^{167}Er^{++}$) and $^{86.5}M$ ($^{173}Yb^{++}$).[10, 17] Finally, analytical results are obtained by the internal mass fractionation correction of Sr given that $^{86}Sr/^{88}Sr$ = 0.1194.[7] Additional bias corrections for Kr baseline suppression caused by LA aerosols were recently introduced for $^{87}Sr/^{86}Sr$ measurements to further improve analytical precision and reproducibility for samples low in Sr (e.g., 300 ppm), for which large amounts of LA aerosols needed to be introduced.[14]

1.2.Analysis of Sr isotope ratios in glass samples

Analysis of the $^{87}Sr/^{86}Sr$ isotope ratio from a small glass sample, such as olivine-hosted small glass inclusions (diameters of 50–200 µm or less), is particularly useful for the identification of the source processes in the genesis of basalt magmas. These glass inclusions can preserve information regarding the primary magma generated in the deep mantle and is unaffected by chemical modifications during ascent to the surface by encapsulation of tiny drops of the deep, quenched magmas.[3, 18] Attempts to analyse a basalt glass were described by Christensen et al. in the first paper published on in situ $^{87}Sr/^{86}Sr$ isotope analysis using LA-MC-ICP-MS, in which they analysed the groundmass glass of Long Valley basalt from a 300-µm/20-Hz crater (approximate sample volume: V = ~2.1 × 10^{-5} cm^3), sampled by an infrared (IR) Nd-YAG laser with

an internal/intermediate precision of $^{87}Sr/^{86}Sr$ = approximately ±0.0005 (two-standard deviation: 2SD).[1]

The attempt continued with development in an ultraviolet 213-nm YAG laser and a third-generation MC-ICP-MS, allowing analysis from a smaller crater of 120-µm/20-Hz (V = ~7.9 × 10^{-7} cm^3) with a similar internal/intermediate precision of approximately ±0.0005 2SD.[3] An alternative approach was to use a sector field (SF)-ICP-MS with rapid peak jumping using a single ion counter (IC) connected to a 193-nm excimer laser (ExLA). This allowed analysis of a smaller sample volume, a crater from 50 µm/10 Hz (V = ~9.8 × 10^{-8} cm^3), with an intermediate precision of approximately ±0.0010 2SD.[19] Analysis of the small sample volume was achieved through use of the high-sensitivity IC, whereas use of the IC with peak jumping resulted in poor intermediate precision.

1.3.Focus

In this study, we present an improved analytical technique for Sr isotope analysis of glass samples. We apply a 193-nm ExLA laser sampling method, with simultaneous introduction of Aridus II solution aerosols (dual intake system),[14] connected to an MC-ICP-MS. In order to prevent any potential oxide interferences, the interface of the MC-ICP-MS was set to achieve the lowest oxide molecular yield.[20] Low instrumental sensitivity with the interface was accounted for by the use of a high-efficiency rotary pump at the interface[14, 20-22] and the application of high-gain Faraday amplifiers using a 10^{12}-Ω resistor.

Use of these amplifiers increases sensitivity by 10 times by reducing the signal-to-noise ratio to half of what would be obtained from an amplifier with a 10^{11}-Ω

resistor. This can in turn reduce analytical error generated during the analysis by more than half for low electron currents.[23, 24] We also examine the Kr baseline-induced bias[14] during loading of smaller samples to the ICP and temporal changes in the Rb overlap correction factor for glass samples with high Rb content. The small sample size and the internal/intermediate precision achieved in this study are keys to the successful application of LA-MC-ICP-MS to small glass inclusions.

2. Instrument setting, data acquisition/reduction

2.1.Laser ablation (LA) and dual-intake sample introduction

The instrumentation for our LA-multiple correction (MC)-ICP-MS has been reported elsewhere for the in situ Sr isotope analysis of plagioclase crystals[14, 15, 25] In brief, the instrument consists of an LA-Aridus II dual-intake system including a 193-nm excimer LA system with a COMPex 102 laser source (Coherent, Göttingen, Germany) combined with an Aridus II desolvating nebuliser (CETAC Technologies, Omaha, USA). The laser aerosols in the He gas flow and the Aridus II solution aerosols in the Ar gas flow were mixed in a T-piece connector just prior to the ICP torch in the MC-ICP-MS. The excimer laser operated with a fluence of 20 J cm^{-2}, a 50–200-µm crater diameter, and, in most cases, a 10-Hz repetition rate, which resulted in craters with depths of ~50 µm after ablation for ~35 s (idle time, 10 s; data acquisition, 25 s), indicating a drilling rate of 0.125-µm per shot.

2.2.MC-ICP-MS

A NEPTUNE MC-ICP-MS was used (Thermo Fisher Scientific, Bremen, Germany) and was modifications at the interface for a high sensitivity as has been reported

elsewhere.[14, 20] The settings of the ion interface were normal (N) Ni sampling and normal (H) Ni skimmer cones with the guard electrode (GE) turned off (electrically disconnected) (**Table 1**). This allowed minimisation of the oxide molecular ion yields ($^{238}U^{16}O^+/^{238}U^+$ < 1%, analysed in solution by Aridus II) and thus, any oxide based interference (e.g., GaO^+) was avoided. The important doubly charged REE ions were monitored by half mass Faradays set at $^{83.5}M$ for $^{167}Er^{++}$ and $^{86.5}M$ for $^{173}M^{++}$ (**Table 1**),[20] and these were almost completely absent (grand averages of the per cent REE^{++} on the most affected ^{84}Sr signals were $^{168}Er^{++}/^{84}Sr$ < 0% and $^{168}Yb^{++}/^{84}Sr$ = 0.004 %; calculations from **ESI Data Table 1**†) for glass samples.

With the interface designed to maintain low oxide levels, as noted above, the system sensitivity was maintained at 200 V/ppm Sr (~11 Gcps/ppm) measured from the Aridus II solution.[3, 10] Analysis of ~300–400 ppm of Sr in glasses yielded a ^{88}Sr signal of 0.5–0.8 V and ~0.1–0.2 V from 100-µm/10-Hz and 50-µm/10-Hz laser craters, respectively (**ESI Data Table 1**†). These values were sufficient for an internal analytical precision of $^{87}Sr/^{88}Sr$ = ±0.0002 to ~0.0010 (2SE) after ~25 s of data acquisition. This was achieved by the application of high-gain Faraday amplifiers, equipped with 10^{12}-Ω resistors,[23] to all naturally occurring Sr isotopes (^{84}Sr, ^{86}Sr, ^{87}Sr, and ^{88}Sr) and ^{85}Rb (**Table 1**).

2.3.Laser ablation protocol

We especially focused on optimizing the LA analytical protocol for the use of 10^{12} Ω high-gain amplifiers because of their slow response to transient signals.[23, 26] One cycle of data acquisition consisted of: (1) two 30-s baseline measurements made on-peak before laser firing; (2) subsequent firing of the laser for 10 s without data acquisition,

allowing stabilisation of the LA signal and the current applied to the Faraday amplifiers in order to avoid the acquisition of transient signals during LA signal growth; and (3) data acquisition for ~25 s using a time slice of ~0.524 s for 50 scans, completed while the signal output was flat and stable (**Fig. 1**). The detailed setup parameters of the laser system and the MC-ICP-MS, including the Faraday collector setup in the mass spectrometer, are listed in **Table 1**.

2.4.Correction of Rb isobaric overlap

Correction of interference from the ^{87}Rb isobar on ^{87}Sr is particularly important in the precise analysis of glasses because natural basaltic glasses contain Rb in the range 0.02–0.15 or more times the amount of Sr.[19, 27] Previous studies used both synthetic[2] or natural glasses[3, 19] of known contents of Rb and Sr and of known ^{87}Sr/^{86}Sr isotope ratio. This allows determination of the overlap correction factor of Rb by adjusting the ^{85}Rb/^{87}Rb isotope ratios to reproduce the known ^{87}Sr/^{86}Sr isotope ratio of the glasses.

We have been using a different approach for determination of the Rb overlap correction factor, using a LA–Aridus solution aerosol dual-intake system. This system has been applied to Hf, Nd, and Sr isotope analyses of zircon,[28] monazite/apatite and rutile,[20] and plagioclase,[14] respectively. The advantage of this method is its ability to simultaneous fine-tune the MC-ICP-MS instrument for both the solution and the LA aerosols from the dual-intake lines, by using solution aerosols while LA firing is off and the laser cell gas is on. Precise determination of an overlap correction factor (e.g., ^{176}Yb and ^{176}Lu on ^{176}Hf;[28] ^{144}Sm on ^{144}Nd;[20] and ^{87}Rb on ^{87}Sr[14]) is simple by using mixed solutions with known (not necessarily accurate) concentrations of the interfering-interfered elements and known isotope composition.

The tuning solution can easily be prepared by mixing standard solutions. The determined correction factor can be used for the LA aerosols while Aridus II introduces deionised water (DIW). The matrix effect of the concomitant major elements from LA aerosols has been examined by major element-doped solutions[28] or by comparisons to the known TIMS values of the LA analytes.[14, 20, 28] The bias was found to be negligible within the level of intermediate precision of ±0.00002 for Hf (~90-ppm offset in naturally occurring $^{176}Hf/^{177}Hf$), Nd (~40-ppm offset in $^{143}Nd/^{144}Nd$), and Sr (~30-ppm offset in $^{87}Sr/^{86}Sr$) isotope analyses.[14, 20, 28] It should be noted that the majority of these analyses were mostly done with a crater size smaller than 200 µm/20 Hz and with the same instruments used in this study. The effectiveness and stability of Rb overlap correction are discussed in **Section 3.2**, particularly for glass samples high in Rb content.

2.5.Data reduction

First, the peak intensities of ^{84}Sr, ^{86}Sr, ^{87}Sr, ^{88}Sr, and ^{85}Rb were measured using on-peak background subtraction. ^{87}Sr intensity was corrected for ^{87}Rb overlap by using the pre-determined $^{85}Rb/^{87}Rb$ isotope ratio (**Section 2.4**) and the measured ^{85}Rb intensity. $^{84}Sr/^{86}Sr$ and $^{87}Sr/^{86}Sr$ isotope ratios were calculated from the intensities of ^{84}Sr, ^{86}Sr and ^{87}Sr (employing the correction for ^{87}Rb overlap), while ^{88}Sr was determined by the exponential law given that $^{86}Sr/^{88}Sr = 0.1194$. Further Kr baseline bias was corrected by using $^{84}Sr/^{86}Sr$ and $^{87}Sr/^{86}Sr$ ratios with the following equation:

$$^{87}Sr/^{86}Sr_{corrected} = {}^{87}Sr/^{86}Sr_{original} / (-0.14121 \times {}^{84}Sr/^{86}Sr + 1.0081)$$

using the empirical correction coefficients proposed by Kimura et al.[14] The above calculations were applied off-line to all 50 scans in a given run. An average and twice

the standard error (2SE) were calculated for each spot; in this case, all the errors that propagated from each isotope measurement were included in the calculated 2SE, while errors from the Rb overlap correction factor and the coefficients used for Kr baseline bias were not included because of their minimal effect.

Kr bias correction itself does not improve internal or external precision caused by the short or long term drift in Kr baselines, a feature that is described elsewhere for iterative Kr baseline subtraction.[13] The major role of this technique is to account for Kr baseline suppression due to the mass loading of LA aerosols; the improvement in this bias can be as high 250 ppm, which is far greater than the Kr baseline drift.[14] The effect of the Kr baseline bias with regards to this study is discussed in **Section 3.1**.

3. Results

Although the analytical protocol for Sr isotope measurements using LA-MC-ICP-MS has been rigorously examined and researchers have been largely in consensus regarding the analytical protocol, special care must nevertheless be taken with Kr baseline suppressions and the Rb overlap correction. We identified new features of these factors, as described below.

3.1.Kr baseline suppression with varied sample loading

3.1.1. Mass loading and Kr baselines: a basic test

We tested the effect of mass loading of LA aerosols by analysing an ~5 ppb SRM 987 Sr standard solution, along with introduction of LA aerosols at different laser crater sizes obtained from an olivine crystal in a picrite lava from St. Helena Island.[29] The SRM 987 is free from any interference from concomitant elements, while Sr and Rb signals from

the tested olivine were both below the detection limits. Kr outgassing during LA was reported from olivine in the JP-1 peridotite[14] but this was not detected from the olivine in the picrite. The olivine sample is therefore suitable for mass loading tests.

The ^{88}Sr intensity from ~5-ppb SRM 987 was ~0.5 V, which was approximately the same signal size as that from a 100-µm/10-Hz carter on a plagioclase/glass containing ~300-ppm Sr. The SRM 987 solution was first analysed for ^{87}Sr/^{86}Sr without LA firing. Subsequent analyses used 50-µm/10-Hz (rate of LA aerosol loading: Vt = 2.5 × 10^{-9} cm^3 s^{-1}), 100-µm/10-Hz (Vt = 9.8 × 10^{-9} cm^3 s^{-1}), 200-µm/10-Hz (Vt = 3.9 × 10^{-8} cm^3 s^{-1}), and 200-µm/20-Hz (Vt = 7.8 × 10^{-8} cm^3 s^{-1}) craters with increasing loaded mass from the olivine aerosols. The Sr signals vary with different LA aerosol loading when analysing a Sr-bearing material with a different crater size; therefore, the absolute role of Kr baseline suppression cannot be tested, particularly for small aerosol loading due to large internal analytical errors in ^{87}Sr/^{86}Sr (see **Section 3.1.2**).

Analytical results are given in **Fig. 2**. The results show a nonlinear relationship, indicating a small suppression of the Kr baseline with 50–100-µm/10-Hz craters, whereas an obvious increase in the uncorrected Sr isotope ratio occurs in 200-µm/10–20-Hz craters. This confirmed the necessity for correction of the Kr baseline suppression. The first report of this suppression was on a 200-µm/5–10-Hz crater for plagioclase analysis,[14] the necessity of which may have been questioned, but our new analysis clearly demonstrates the necessity of the correction when the sample loading of LA is greater than 3.9 × 10^{-8} cm^3 s^{-1}. Even with a low mass loading, corrected data are closer to the reference value of SRM 987, indicating the importance of this bias correction (**Fig. 2**).

The baseline bias correction with the heaviest sample loading at 7.8 × 10^{-8} cm^3

s^{-1} from a 200-μm/20-Hz crater appears to be invalid, showing a large offset in the corrected Sr isotope ratio (**Fig. 2**). In this particular analysis, we saw ~10% suppression of the ^{88}Sr signal for the SRM 987 solution during loading of the olivine LA aerosols, suggesting suppression of Sr in the ICP (not shown). This was not observed with the smaller sample loading. The nonlinear response of the Sr signal might originate from the nonlinear response described by Saha's equation[30, 31] where an increase in the electron number density causes a sigmoidal decrease of the ionisation efficiency.[21, 30-32] Sr signal suppression relative to Kr was not taken into account for the Kr baseline bias correction in the previous paper;[14] therefore, the proposed correction could apply only to the LA aerosol loading smaller than 7.8×10^{-8} cm^3 s^{-1} with the 200-μm/20-Hz crater used in this study. The effect of signal suppression is discussed further in **Section 3.2.1**.

3.1.2. Effect of Kr baseline suppression in plagioclase analysis

We conducted a series of experiments using an extremely homogeneous anorthite plagioclase MkAn.[14, 25] The Sr isotope composition of the crystal is homogeneous, ^{87}Sr/^{86}Sr = 0.70345 ± 0.00002 (error in 2SD, n = 4) confirmed by TIMS and LA-MC-ICP-MS.[14, 25] This crystal contains minuscule amounts of Rb (0.07 ppm), with Sr = 305 ppm[21] and thus it is the best suited for examination of the Kr baseline suppression without considering the effect of Rb overlap.

Using the MkAn, analyses of Sr isotope ratios were performed with ablation conditions of 200 μm/20 Hz, 200 μm/10 Hz, 100 μm/10 Hz, and 50 μm/10 Hz (**Fig. 3a** and **ESI Data Table 1**†). We rearranged the data using the Kr baseline bias uncorrected data of ^{87}Sr/^{86}Sr and ^{84}Sr/^{86}Sr based on the crater size (**Fig. 3b**). The data from the 200-μm/10–20-Hz plot on the same negatively sloped linear regression line, which is

sub-parallel to the theoretical fractionation line of Kr baseline suppression proposed by the previous study.[14] The amount of LA aerosols from a 200-μm/20-Hz crater is about 0.7 times smaller than that from olivine because of the poorer coupling of 193-nm excimer laser light to the transparent (Fe- and Mg-poor) plagioclase. This would be the reason for the lack of offset from the Kr baseline bias for this sample amount. In contrast, the regression lines of the 100 μm/10 Hz and 50 μm/10 Hz data are sub-parallel, but with shallower slopes than those from 200-μm craters. Kr baseline corrections, made by the theoretical model of Kimura et al.,[14] resulted in an almost flat regression line for the data from 200-μm craters (**Fig. 3c**), indicating almost perfect correction of the bias. The same correction made for the data from 100–50-μm craters showed slight over-reductions as shown by the positively sloped regression lines in **Fig. 3c**.

This examination clearly indicates that the Kr baseline suppression is due to mass loading of the plagioclase aerosols, but the degree of suppression could be nonlinear against the amount of aerosol loaded. The mass loading from 200-μm craters clearly showed the bias, whereas 50–100-μm craters showed the same bias, but to an apparently smaller extent. The systematic errors from the potential nonlinearity, deduced from the slopes of the regression lines of 50–100-μm craters, are well within the typical internal precision of ±0.0002 for these small craters both before and after the bias corrections (**Fig. 3b** and **3c**). Therefore, we corrected for the baseline bias even for the small 50–100-μm craters. As shown, the $^{87}Sr/^{86}Sr$ form SRM 987 solution showed a closer match to the reference value after the bias correction for a small aerosol loading (**Fig. 2**), which also supports our approach. The analytical results of MkAn are given in **Fig. 3a** and **ESI Data Table 1**†, and show an almost perfect match with the isotope

ratios measured by TIMS ($^{87}Sr/^{86}Sr$ = 0.70345 ± 0.00002) for all sample sizes; 0.7035 ± 0.0002, 2SD, n = 26, 200-µm craters; 0.7034 ± 0.0002, 2SD, n = 10, 100-µm craters; and 0.7035 ± 0.0008, 2SD, n = 40, 50-µm craters.

3.2.Rb overlap correction factor and its temporal drift

3.2.1. Determination of the Rb correction factor

We determined the $^{85}Rb/^{87}Rb$ correction factor using the dual-intake system over the period of analyses of this study and found a temporal change of the value obtained (**Fig. 4a** and **4b**). The correction factor was obtained by analysing an ~5-ppb NIST SRM 987 standard solution ($^{87}Sr/^{86}Sr$ = 0.71024)[27] doped with an ~1-ppb Rb, in which Rb/Sr = ~0.2 is higher than all target glasses. The acquisition was done by the same protocol as for the LA analysis but with a longer time slice of ~4.25 s for 50 scans in order to obtain high-precision results. In this measurement, instrumental mass fractionation of Sr was determined by a stable isotope ratio of $^{86}Sr/^{88}Sr$ = 0.1194.[33] The mass fractionation was corrected by the exponential law for both Sr and Rb isotope ratios, assuming the same mass fractionation factor over the mass range ^{84}M–^{88}M. This calculation protocol is the same as that used for the LA analyses.

We determined the $^{87}Sr/^{86}Sr = S_1$ ratio of the mixed solution with a provisional $^{85}Rb/^{87}Rb$ value (e.g., 2.5926, the canonical value of $^{85}Rb/^{87}Rb$ from the IUPAC isotopic abundances of ^{85}Rb = 72.165 and ^{87}Rb = 27.835).[33] The obtained $^{87}Sr/^{86}Sr$ was always incorrect because of the difference between the proper and the given $^{85}Rb/^{87}Rb$ ratio, due to the different elemental sensitivity between Rb and Sr, which altered the ratio of $^{87}Rb/^{87}Sr$ (see the similar example between Sm and Nd).[20, 34] The second cycle of the calculation was done using the same analytical data with a different $^{85}Rb/^{87}Rb$ value

(e.g., 2.470) to obtain the second $^{87}Sr/^{86}Sr = S_2$ ratio. The correct $^{85}Rb/^{87}Rb = R_{Rb}$ ratio should be on the linear regression line passing through the coordinates (X, Y) = (S_1, 2.5926) and (S_2, 2.470), obtaining R_{Rb} at (0.70124, R_{Rb}) for the Rb doped SRM 987 standard solution. R_{Rb} does not represent its natural value but represents the value including the correction factor (see the similar example between Lu, Yb, and Hf).[28]

3.2.2. Possible origin of enhanced Rb correction factor

The averaged $R_{Rb} = {}^{85}Rb/^{87}Rb$ value on Day 5 was 2.4688 (**Fig. 4b**), expressed as a mass fractionation factor of ΔM(Rb) = 2.417% in comparison to the canonical value of $^{85}Rb/^{87}Rb$ = 2.5926.[33] This fractionation factor is systematically larger than that measured for $^{86}Sr/^{88}Sr$ which gave ΔM(Sr) = 2.317% assuming $^{86}Sr/^{88}Sr$ = 0.1194 (**Fig. 4c**). This is due to the difference in elemental sensitivity between Rb and Sr as noted in **Section 3.2.1**, showing a 4.35% enhancement of Rb relative to Sr. Note that the ΔM(Rb) values in **Fig. 4c** are derived from the measured and interpolated values shown in **Fig. 4b**; the values have therefore been corrected for temporal drift (see **Section 3.2.3**).

The enhanced ΔM(Rb) values are consistent with the higher ionisation efficiency of Rb than Sr in the ICP, where the first ionisation energy of Rb (640 kJ mol^{-1}) is lower than Sr (660 kJ mol^{-1}), and the boiling and dissociation temperatures of Rb (312.2 and 961 K, respectively) are both lower than those of Sr (1042 and 1657 K, respectively) promoting together the higher ionization efficiency of Rb than for Sr.[35] When the local plasma equilibrium of Saha's equation[30, 31] and electron number density $ne = 1.47 \times 10^{20}$ m^{-3} are assumed, plasma temperature at T = 5514 K is calculated to yield a 4.35% enhancement in the ionization efficiency of Rb (92.05%) relative to Sr (88.21%). This temperature is far lower than that of a standard ICP (T = 6680 K),[36] but

is still similar to the apparent ionization temperature (T = ~5500 K) estimated for element fractionation between a refractory SRM 612 glass and a more easily ionized BCR-2G basalt glass (see Fig. 2F in Kimura and Chang).[21] The large particle size of LA aerosols (10–500-nm with ~100-nm median diameter)[21, 37] and short transit time in the ICP may be the source of this apparently low ionization temperature.[21]

It is worth noting that the ^{85}Rb/^{87}Rb factor determined by the solution aerosols should differ from that for the LA aerosols owing to the change in the plasma conditions when mass loading of the LA aerosols occurs.[21, 32] This was not the case with the volume of LA aerosols and the internal/intermediate precision being dealt with in this study, or in our previous studies, as shown by the intermediate level of analytical precision of the standard materials (**Sections 3.1.1** and **3.3**). In the case of heavy mass loading, however, determination of the ^{85}Rb/^{87}Rb factor by LA aerosols should be recommended.

Finally, the clear correlation between ΔM(Rb) and ΔM(Sr) (**Fig. 4c**) confirms that the Rb overlap correction factor of ^{85}Rb/^{87}Rb, no matter the determination method, should be used in combination with the ^{86}Sr/^{88}Sr mass fractionation factor in each analytical run (see **Section 1.1**) Nevertheless, temporal drift in the Rb correction factor occurs regardless (**Fig. 4b**), and should be closely monitored, determined, and applied (**Section 3.2.3)**.

3.2.3. Temporal drift of Rb correction factor

The ^{85}Rb/^{87}Rb correction factor drifted with time, most likely reflecting a temporal change in elemental sensitivity between Rb and Sr. The general trend showed a rapid increase in ^{85}Rb/^{87}Rb with time after the plasma was on (**Fig. 4a**). The drift stabilised

after 2–3 h but problematic changes could have occurred (see Days 5 and 7 in **Fig. 4a**). The absolute $^{85}Rb/^{87}Rb$ value changed with different sampler and skimmer cones as shown for Days 7 and 8 in **Fig. 4a**. In more detail, the change showed a continuous increase from 2.4669 to 2.4706 and dropped to 2.4694 between runs 39 and 40, followed by a further increase to 2.4698 on Day 5 (**Fig. 4b**). The sudden drop correlates to a longer interval of 1 h with no introduction of LA aerosols. We interpreted the increase in the ratio as being caused by the change in the surface conditions of the interface cones. This daily trend is common to all examples and is significant when using a new sampler-skimmer cone for the first time (Day 7 in **Fig. 4b**). It is likely that the systematic difference between the cones (Day 5–6 and Day 7–8 in **Fig. 4a**) results from their different geometries.

The change of the $^{85}Rb/^{87}Rb$ factor from 2.4669 to 2.4706 causes a systematic bias increase of $^{87}Sr/^{86}Sr$ = 0.0014 for BCR-2G (337-ppm Sr, 48.5-ppm Rb, Rb/Sr = 0.144) and $^{87}Sr/^{86}Sr$ = 0.0002 for BHVO-2G (396-ppm Sr, 9.2-ppm Rb, Rb/Sr = 0.023). Considering the temporal change of the factor, frequent measurement of $^{85}Rb/^{87}Rb$ is crucial for glass samples with a high Rb content. We used the same, ~5-ppb Sr SRM 987 solution doped with ~1-ppb Rb for this purpose and determined the $^{85}Rb/^{87}Rb$ factors for every five unknown LA analyses. The temporal change in $^{85}Rb/^{87}Rb$ was the linearly interpolated for the five unknown calculations.

3.3. Analyses of basalt glass samples

With the instrument settings and the analytical protocols described in the above sections, we then analysed the BHVO-2G, KL2-G, ML3B-G, and BCR-2G glasses, which have also been analysed in the previous LA-ICP-MS studies[18, 19] and TIMS reference values

are thus available.[27]

The basalt glasses of BHVO-2G (basalt from the Hawaiian Volcano Observatory), KL2-G (from Kilauea volcano), and ML3B-G (from Mauna Loa volcano) are all from the Big Island of Hawaii. As shown in **Table 2** and **ESI Data Table 1**†, the results of BHVO-2G were: $^{87}Sr/^{86}Sr$ = 0.70345 ± 0.00020 (n = 15) from 100-µm/10-Hz craters and 0.7035 ± 0.0005 (n = 55) from 50-µm/10-Hz craters, for the TIMS value of $^{87}Sr/^{86}Sr$ = 0.703469 ± 0.000010 (**Fig. 5a**); those of KL2-G were: $^{87}Sr/^{86}Sr$ = 0.70352 ± 0.00013 (n = 5) from 100-µm/10-Hz craters for the TIMS value of 0.703517 ± 0.00002; and those of ML3B-G were: $^{87}Sr/^{86}Sr$ = 0.70386 ± 0.00027 (n = 10) from 100-µm/10-Hz craters for the TIMS value of 0.703805 ± 0.000020. The LA results are all in excellent agreement with the TIMS values, indicating that the appropriate correction factor was used in this study.

BCR-2G (Columbia River Basalt) glass, with Rb/Sr = 0.144, is the most difficult sample for analysis of the isobaric corrections of the concomitant Rb in this study. The results of BCR-2G also showed excellent agreement with the TIMS reference value of $^{87}Sr/^{86}Sr$ = 0.705000 ± 0.000020,[27] as shown by $^{87}Sr/^{86}Sr$ = 0.70495 ± 0.00040 (n = 39) from 100-µm/10-Hz craters and $^{87}Sr/^{86}Sr$ = 0.7051 ± 0.0008 (n = 50) from 50-µm/10-Hz craters (**Fig. 5b**). This proves that the method can be applied to many natural basalt melts of interests.[3]

The intermediate precisions were ±0.00010 for 200-µm/10-Hz craters, ±0.00013–0.00040 for 100-µm/10-Hz craters, and ±0.00050–0.00080 for 50-µm/10-Hz craters (**Table 2** and **Fig. 5**). These internal/intermediate precisions are a factor of approximately two smaller than those obtained by LA-SF-ICP-MS for a 50-µm/10-Hz crater in year 2009.[18, 19] The intermediate precisions of ±0.00050–0.00080 for a

50-µm/10-Hz crater are comparable to those obtained for a 120-µm/20-Hz crater using 216-nm YAG-LA-MC-ICP-MS in year 2006[3] but from an ~10 times smaller sample volume. If compared with the first report of 1064 nm by YAG-LA-MC-ICP-MS in year 1995,[1] the necessary sample amount for a ±0.00010 internal/intermediate precision is ~200 times smaller, reflecting significant improvements in both the instruments and the analytical protocols. These improvements are useful for the analyses of small melt inclusions.

4. Conclusions

We evaluated analytical protocols using LA-MC-ICP-MS for accurate Sr isotope analysis of small glass samples. The Kr baseline suppression during LA analysis was found to be nonlinear; small for small sample aerosol loading and large for an extreme sample loading. We corrected the baseline bias for the all sample amounts from the LA crater of 50–200 µm/10 Hz and found it to be applicable over the range. Precise Rb overlap correction using a Rb-doped standard solution and temporal variation of the correction factor were also examined. The results showed that frequent measurement of the correction factor was required for a high Rb content basalt glass. These correction methods were applied to the in situ Sr isotope analyses of the basalt glass standards of BHVO-2G, BCR-2G, KL2-G, and ML3B-G. The internal/intermediate precisions achieved for the glass standards were $^{87}Sr/^{86}Sr$ = ±0.00010 (200 µm/10 Hz) to 0.00080 (50 µm/10 Hz), dependent on the crater size and Rb content. The results were a factor of two more precise than the previous method using a 50-µm crater with ExLA-SF-ICP-MS and were achieved with a ten times smaller sample volume than those in 213-nm Nd-YAG-MC-ICP-MS. The results demonstrate the wide application of

this method to many naturally occurring melt inclusions in olivine, which typically have a diameter of 30–200 µm with Sr levels of 200–300 ppm.

Acknowledgments

The authors wish to thank Dr Y. Tatsumi of JAMSTEC (currently at Kobe University) for his generous support of this project. We are grateful to Prof. K. P. Jochum of the Max Plank Institute for Chemistry for providing the MPI-DING glasses. The technical and engineering support of Mr K. Ohki of OK Laboratory enabled the manufacture of the high-quality 193-nm excimer LA imaging optics that helped establish the prolonged stable ablation of plagioclase. Discussions with Dr D. Bouman of Thermo Scientific were useful for application of the high-gain amplifiers. Finally, the authors are indebted to the two anonymous reviewers who provided detailed and constructive comments, which helped to further improve this paper.

References

1. J. N. Christensen, A. N. Halliday, D.-C. Lee and C. M. Hall, *Earth and Planetary Science Letters*, 1995, **136**, 79-85. DOI: 10.1016/0012-821x(95)00181-6.
2. J. Davidson, F. Tepley III, Z. Palacz and S. Me¡an-Main, *Earth and Planetary Science Letters*, 2001, **184**, 427-442.
3. M. G. Jackson and S. R. Hart, *Earth and Planetary Science Letters*, 2006, **245**, 260-277. DOI: 10.1016/j.epsl.2006.02.040.
4. T. Takahashi, Y. Hirahara, T. Miyazaki, B. S. Vaglarov, Q. Chang, J.-I. Kimura and Y. Tatsumi, *JAMSTEC Report R&D*, 2009, **Special Issue**, 59-64.
5. M. McCulloch, M. Cappo, J. Aumend and W. Müller, *Marine and Freshwater Research*, 2005, **56**, 637-644. DOI: org/10.1071/MF04184.
6. J. Woodhead, S. Swearer, J. Hergt and R. Maas, *Journal of Analytical Atomic Spectrometry*, 2005, **20**, 22-27.
7. P. Z. Vroon, B. van der Wagt, J. M. Koornneef and G. R. Davies, *Analytical and Bioanalytical Chemistry*, 2008, **390**, 465-476, doi:

410.1007/s00216-00007-01742-00219.

8. R. Barnett-Johnson, F. C. Ramos, C. B. Grimes and R. B. MacFarlane, *Canadian Journal of Fisheries and Aquatic Sciences*, 2005, **62**, 2425-2430. DOI: 10.1139/f05-194.

9. M. Bizzarro, A. Simonetti, R. K. Stevenson and S. Kurszlaukis, *Geochimica et Cosmochimica Acta*, 2003, **67**, 289-302. DOI: 10.1016/s0016-7037(02)01048-7.

10. F. C. Ramos, J. A. Wolff and D. L. Tollstrup, *Chemical Geology*, 2004, **211**, 135-158. DOI: 10.1016/j.chemgeo.2004.06.025.

11. S. S. Schmidberger, A. Simonetti and D. Francis, *Chemical Geology*, 2003, **199**, 317-329. DOI: 10.1016/s0009-2541(03)00125-6.

12. T. Waight, J. Baker and D. Peate, *International Journal of Mass Spectrometry*, 2002, **221**, 229-244. DOI: 10.1016/s1387-3806(02)01016-3.

13. J. G. Konter and L. P. Storm, *Chemical Geology*, 2014, **385**, 26-34. DOI: 10.1016/j.chemgeo.2014.07.009.

14. J.-I. Kimura, T. Takahashi and Q. Chang, *Journal of Analytical Atomic Spectrometry*, 2013, **28**, 945-957. DOI: 0.1039/c3ja30329b.

15. Y. Tatsumi, T. Takahashi, Y. Hirahara, Q. Chang, T. Miyazaki, J.-I. Kimura, M. Ban and A. Sakayori, *Journal of Petrology*, 2008, **49**, 1971-2008.

16. J.-I. Kimura, Q. Chang, K. Itano, T. Iizuka, S. B. Vaglarov and K. Tani, *Journal of Analytical Atomic Spectrometry*, 2014. DOI: 10.1039/C4JA00257A.

17. Y. H. Yang, H.-Y. Wu, J.-H. Yang, D. M. Chew, L.-W. Xie, Z.-Y. Chu, Y.-B. Zhang and C. Huang, *Chemical Geology*, 2014, **385**, 35-55. DOI: 10.1016/j.chemgeo.2014.07.012.

18. A. V. Sovolev, A. W. Hofmann, K. P. Jochum, D. V. Kuzmin and B. Stoll, *Nature*, 2011, **476**, 434-437. DOI: 10.1038/nature10321.

19. K. P. Jochum, B. Stoll, U. Weis, D. V. Kuzmin and A. V. Sovolev, *Journal of Analytical Atomic Spectrometry*, 2009, **24**, 1237-1243. DOI: 10.1039/b905045k.

20. J.-I. Kimura, Q. Chang and H. Kawabata, *Journal of Analytical Atomic Spectrometry*, 2013, **28**, 1522-1529. DOI: 10.1039/c3ja50109d.

21. J. I. Kimua and Q. Chang, *Journal of Analytical Atomic Spectrometry*, 2012, **27**, 1549-1559. DOI: 10.1039/c2ja10344c.

22. C. Bouman, M. Deerberg and J. B. Schwieters, *Application Note Thermo Scientific*, 2009, **30187**, 1-4.

23. J. M. Koornneef, C. Bouman, J. B. Schwieters and G. R. Davies, *Journal of Analytical Atomic Spectrometry*, 2013, **28**, 749-754.

24. J.-I. Kimura, T. Nozaki, S. R. and K. Suzuki, *Journal of Analytical Atomic*

Spectrometry, 2014, DOI: 10.1039/c1034ja00092g.

25. T. Takahashi, Y. Hirahara, T. Miyazaki, R. Senda, Q. Chang, J.-I. Kimura and Y. Tatsumi, *Journal of Petrology*, 2012. DOI: 10.1093/petrology/egs065.

26. T. Hirata, Y. Hayano and T. Ohno, *Journal of Analytical Atomic Spectrometry*, 2003, **18**, 1283-1288.

27. K. P. Jochum, U. Nohl, K. Herwig, E. Lammel, B. Stoll and A. W. Hofmann, *Geostandards and Geoanalytical Research*, 2005, **29**, 333-338.

28. J.-I. Kimura, K. Tani and Q. Chang, *Geochemical Journal*, 2012, **46**, 1-12.

29. H. Kawabata, T. Hanyu, Q. Chang, J.-I. Kimura, A. R. L. Nichols and Y. Tatsumi, *Journal of Petrology*, 2011, **52**, 791-838.

30. H. Bradt, in *Astrophysics Processes*, Cambridge University Press, Cambridge. 2008, p. 536.

31. M. N. Saha, *Nature*, 1920, **105**, 232-233.

32. I. Kroslakova and D. Günther, *Journal of Analytical Atomic Spectrometry*, 2007, **22**, 51-62.

33. International_Union_of_Pure_and_Applied_Chemistry, *Pure & Applied Chemistry*, 1984, **56**, 695-768.

34. T. Iizuka, S. M. Eggins, M. T. McCulloch, L. P. J. Kinsley and G. E. Mortime, *Chemical Geology*, 2011, **282**, 45-57. DOI: 10.1016/j.chemgeo.2011.01.008.

35. J. Emsley, *The Elements*, Clarendon Press, Oxford. 1998.

36. G. Horlick and Y. Shao, in *Inductively Coupled Plasma in Analytical Atomic Spectrometry 2nd ed.*, ed. A. Montaster and D. W. Golightly, VCH Pub. Inc., New York. 1992, p. 564.

37. F.-X. D'Abzac, A.-M. Seydoux-Guillaume, J. Chmeleff, L. Datas and F. Poitrasson, *Journal of Analytical Atomic Spectrometry*, 2012, **27**, 108-119. DOI: 10.1039/c1ja10145d.

Figure and Table caption

Fig. 1. Signal profiles (a) and isotope ratios (b) acquired from a 50-µm crater in ~25 s on BCR-2G. Stable signals and isotope ratios are obtained after 10 s of idle time with laser firing. No effect from slow response of the Faraday amplifiers was observed.

Fig. 2. Variation of $^{87}Sr/^{86}Sr$ of SRM 987 solution (~0.5-V ^{88}Sr) measured with various amounts of aerosol loading from a St Helena olivine crystal. The bias from Kr baseline suppression is significant in the crater size 200 µm/20 Hz. Uncorrected values are from isobaric overlap and mass fractionation corrections only. Corrected values are further corrected for Kr baseline-induced bias. Errors are in 2SE. Aerosol loading without LA (w/o LA) is provisionally plotted at 1×10^{-9} cm^3 s^{-1}.

Fig. 3. Analytical results of the MkAn anorthite using different crater sizes for different amounts of sample aerosol loading (panel a). Uncorrected (panel b) and corrected $^{87}Sr/^{86}Sr$–$^{84}Sr/^{86}Sr$ ratios (panel c) of the Kr baseline-induced biases are compared for the different sample volumes. Data from large volume aerosols (200-µm/10–20-Hz crater) is plotted on the theoretical fractionation line of the Kr baseline suppression, while those from the smaller volume aerosols (100–50-µm/10-Hz craters) show slight over-corrections. Potential biases from these overcorrections are less than ±0.00020 (thick vertical line), well below the in-run analytical precisions for these data. Thick shaded lines, thin solid lines, and thin dotted lines are regression lines for the results from 200-, 100-, and 50-µm craters, respectively. Thin dashed lines show the reference value of the MkAn as measured by TIMS.

Fig. 4. Daily temporal variations of $^{85}Rb/^{87}Rb$ correction factors during analyses of basalt glass samples (panel a). The large gap between runs 39 and 40 is due to a long break for 2 h indicating reverse shift of the drift due to no loading of the laser aerosols (panel b). Apparent Rb mass bias and actual Sr mass bias, measured on Day 5 (panel c). Note that open squares show measured values and dots are interpolations in panel b. See details in the text.

Fig. 5. Analytical results of BHVO-2G and BCR-2G glass standards. Internal precisions are given by 2SE, whereas those for averages (open circles) are given by two-standard deviation (2SD). Solid squares and shaded lines are TIMS reference values.

Table 1. Laser and mass spectrometer set-up parameters for the LA-MC-ICP-MS Sr isotope analysis

Table 2. Representative LA-MC-ICP-MS analytical results of Sr isotope ratios in synthetic glass standards

ESI Data Table 1. LA-MC-ICP-MS analytical results of Sr isotope ratios

Table of Contents Entry: Graphical abstract

An analytical protocol using LA-MC-ICP-MS for precise Sr isotope ratio analysis from small glass samples is presented

Table 1. Laser and mass spectrometer set-up parameters for the LA-MC-ICP-MS Sr isotope analysis

Apparatus	Experimental setting	
Excimer laser	OK Laboratory Ltd. (in house)	
Source wave length/pulse width	193 nm/20 ns	
Energy at source	200 mJ	
Focusing lens	Imaging optics using field lens and air spaced doublet objective	
Spot size	50, 100, and 200 μm	
Fluence at laser spot	20 J cm^{-2}	
Repetition rate	10 and 20 Hz	
Aridus II	CETAC Technologies	
Spray chamber temperature	110 °C	
Membrane temperature	160 °C	
Nebuliser flow	1.0 L min^{-1}	
Membrane gas flow	~3.5 L min^{-1}	
Additional N_2 gas flow	1.5 mL min^{-1}	
MC-ICP-MS	Thermo NEPTUNE	
RF-power	1400 W	
Guard electrode	off (electronically disconnected)	
Sampling cone	N-sample cone (Ni)	
Skimmer cone	N-skimmer cone (Ni)	
Plasma gas (Ar)	1.0 L min^{-1}	
Laser carrier gas (He)	0.7 L min^{-1}	
Interface vacuum with E2M80	1.7 mbar with He ablation carrier gas	
Acquisition time	0.5 s × 50 scans for LA and 4 s × 50 scans for solution	
Faraday detector setting		
^{83}Kr (^{83}Kr, ^{43}Ca^{40}Ca, ^{43}Ca^{40}Ar)	FC L4	(10^{11}Ω amplifier)
$^{83.5}$M (^{167}Er^{++})	FC L3	(10^{11}Ω amplifier)
^{84}Sr (^{84}Kr, ^{44}Ca^{40}Ca, ^{44}Ca^{40}Ar)	FC L2	(10^{12}Ω amplifier)
^{85}Rb (^{85}GaO)	FC L1	(10^{12}Ω amplifier)
^{86}Sr (^{86}Kr, ^{46}Ca^{40}Ca, ^{46}Ca^{40}Ar)	FC Center	(10^{12}Ω amplifier)
$^{86.5}$M (^{173}Yb^{++})	FC H1	(10^{11}Ω amplifier)
^{87}Sr (^{87}Rb, ^{85}GaO)	FC H2	(10^{12}Ω amplifier)
^{88}Sr (^{48}Ca^{40}Ca, ^{48}Ca^{40}Ar)	FC H3	(10^{12}Ω amplifier)
Background subtraction	on peak background subtraction	

FC: Faraday cup; isobaric atomic and molecular ions are shown in parentheses

Table 2. Representative LA-MC-ICP-MS analytical results of Sr isotope ratios in synthetic glass standards

Sample	Sr	Rb	Rb/Sr	$^{87}Sr/^{86}Sr$	2SD	n	$^{87}Sr/^{86}Sr$	2SD	n	$^{87}Sr/^{86}Sr$	2SE	Reference
	ppm	ppm		LA-ICP-MS (100 µm)			LA-ICP-MS (50 µm)			TIMS	(GeoREM)	
BHVO-2G	396	9.2	0.023	0.70345	0.00020	15	0.7035	0.0005	55	0.703469	0.00001	This study
				–	–	–	0.7035	0.0010	36	–	–	Jochum et al. (2009)
				–	–	–	0.7035	0.0010	–	–	–	Sovolev et al. (2011)
KL2-G	356	8.7	0.024	0.70352	0.00013	5	–	–	–	0.703517	0.00002	This study
				–	–	–	0.7036	0.0008	43	–	–	Jochum et al. (2009)
				–	–	–	0.7035	0.0008	–	–	–	Sobolev et al. (2011)
ML3B-G	312	5.8	0.019	0.70386	0.00027	10	–	–	–	0.703805	0.00002	This study
				–	–	–	0.7038	0.0008	48	–	–	Jochum et al. (2009)
				–	–	–	0.7038	0.0010	–	–	–	Sobolev et al. (2011)
BCR-2G	337	48.5	0.144	0.70495	0.00040	39	0.7051	0.0008	50	0.705000	0.00002	This study

Note: 2SD = two-standard deviation; 2SE = two-standard error; n = number of analyses. TIMS reference values are from GeoREM[27]

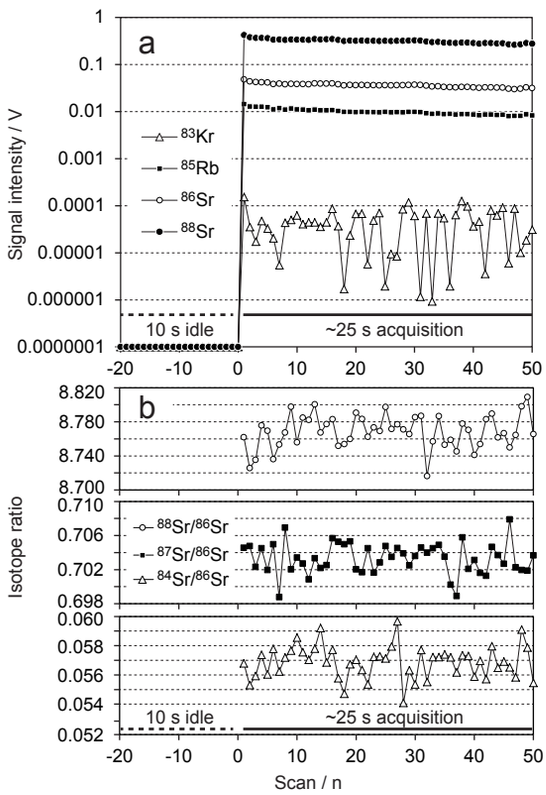

Fig. 1.

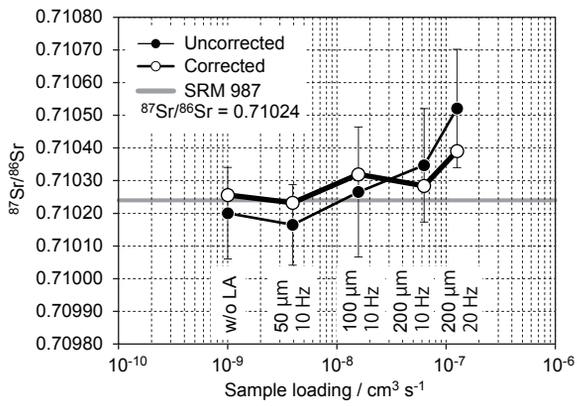

Fig. 2.

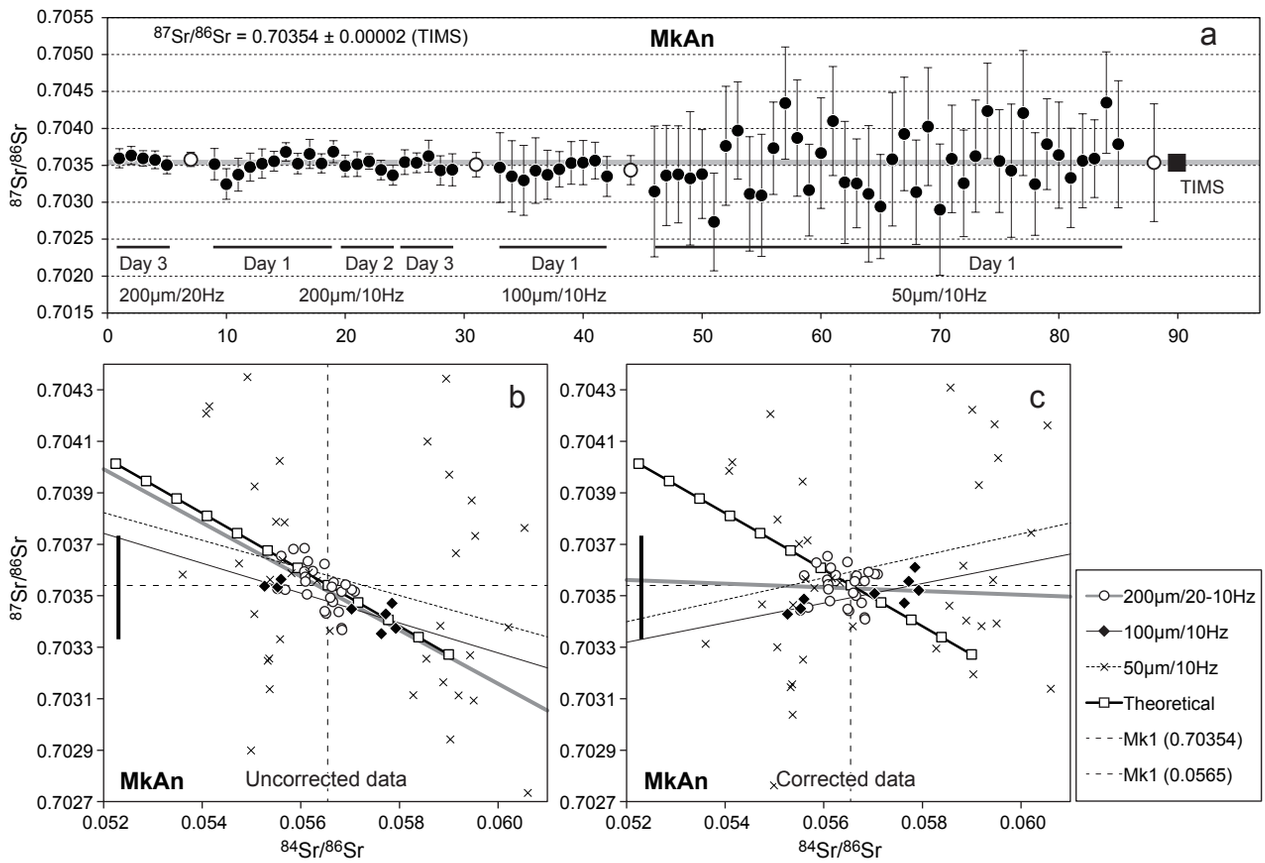

Fig. 3.

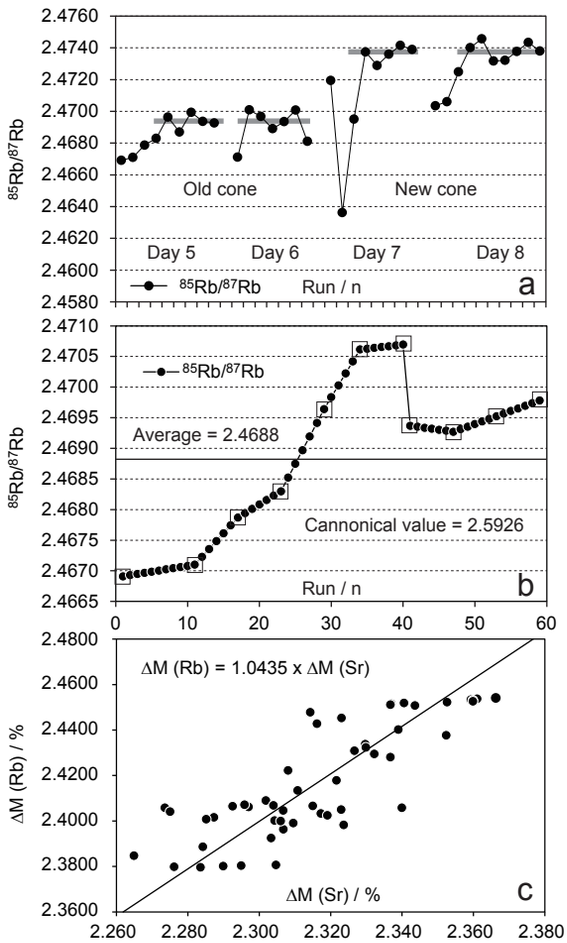

Fig. 4.

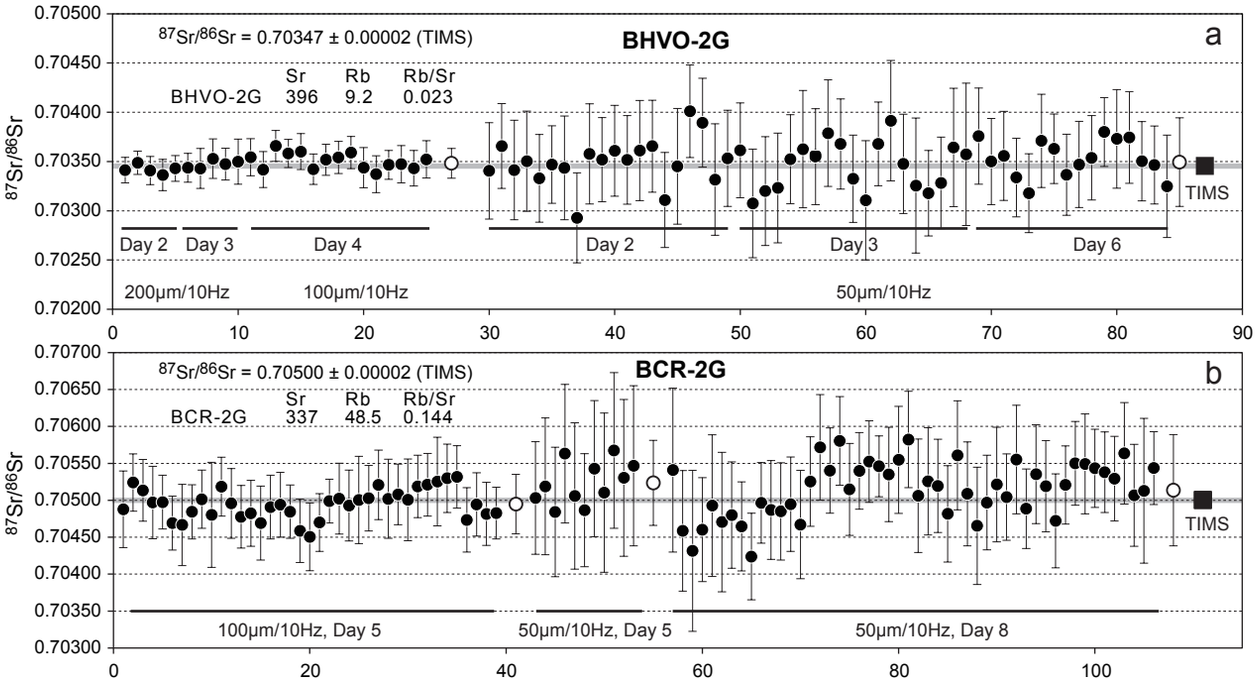

Fig. 5.

E.S.I. Data Table 1 Analytical results of Sr isotope ratios

Day	Run ID	Crater	Sample	^{83}Kr (V)	$^{83.5}$M (V)	^{84}Sr (V)	^{85}Rb (V)	^{86}Sr (V)	$^{86.5}$M (V)	^{87}Sr (V)	^{88}Sr (V)	^{84}Sr/^{86}Sr	^{87}Sr/^{86}Sr	^{88}Sr/^{86}Sr	^{87}Sr/^{86}Sr cor	2SE
JUL 26 2014	Run5	200um/20Hz	MkAn1_1	0.00117	-0.00001	0.01178	0.00004	0.21948	-0.00002	0.15805	1.92449	0.05624	0.70360	8.76804	0.70352	0.00013
JUL 26 2014	Run6	200um/20Hz	MkAn1_2	0.00133	0.00001	0.01286	0.00006	0.24015	-0.00001	0.17297	2.10626	0.05614	0.70363	8.77060	0.70355	0.00012
JUL 26 2014	Run7	200um/20Hz	MkAn1_3	0.00154	-0.00001	0.01445	0.00008	0.27020	-0.00001	0.19460	2.36967	0.05607	0.70359	8.76992	0.70350	0.00010
JUL 26 2014	Run8	200um/20Hz	MkAn1_4	0.00180	-0.00001	0.01642	0.00074	0.30698	0.00000	0.22138	2.69283	0.05609	0.70357	8.77176	0.70348	0.00012
JUL 26 2014	Run9	200um/20Hz	MkAn1_5	0.00119	0.00000	0.01175	0.00005	0.21935	0.00000	0.15794	1.92321	0.05613	0.70351	8.76742	0.70342	0.00012
Average and error in 2SD													**0.70358**	**0.00009**	**0.70349**	**0.00010**
JUL 24 2014	Run8	200um/10Hz	MkAn1_1	0.00028	0.00000	0.00565	0.00003	0.10349	0.00000	0.07445	0.90576	0.05710	0.70352	8.75227	0.70352	0.00021
JUL 24 2014	Run9	200um/10Hz	MkAn1_2	0.00026	-0.00001	0.00518	0.00003	0.09405	0.00000	0.06760	0.82241	0.05762	0.70325	8.74408	0.70330	0.00021
JUL 24 2014	Run10	200um/10Hz	MkAn1_3	0.00024	-0.00001	0.00477	0.00003	0.08776	-0.00001	0.06311	0.76786	0.05683	0.70337	8.74932	0.70335	0.00022
JUL 24 2014	Run11	200um/10Hz	MkAn1_4	0.00026	0.00000	0.00518	0.00003	0.09558	-0.00001	0.06875	0.83626	0.05665	0.70348	8.74836	0.70344	0.00019
JUL 24 2014	Run12	200um/10Hz	MkAn1_5	0.00026	0.00000	0.00506	0.00004	0.09280	0.00000	0.06674	0.81166	0.05703	0.70352	8.74643	0.70352	0.00020
JUL 24 2014	Run38	200um/10Hz	MkAn1_31	0.00040	0.00000	0.00835	0.00010	0.15556	0.00000	0.11188	1.36001	0.05609	0.70355	8.74162	0.70346	0.00013
JUL 24 2014	Run39	200um/10Hz	MkAn1_32	0.00040	0.00001	0.00848	0.00005	0.15871	0.00000	0.11416	1.38802	0.05585	0.70368	8.74544	0.70357	0.00012
JUL 24 2014	Run40	200um/10Hz	MkAn1_33	0.00038	-0.00002	0.00827	0.00004	0.15527	0.00000	0.11166	1.35790	0.05568	0.70352	8.74486	0.70339	0.00014
JUL 24 2014	Run41	200um/10Hz	MkAn1_34	0.00042	0.00000	0.00868	0.00005	0.16319	-0.00001	0.11737	1.42700	0.05560	0.70365	8.74416	0.70352	0.00020
JUL 24 2014	Run42	200um/10Hz	MkAn1_35	0.00041	-0.00001	0.00859	0.00005	0.16161	-0.00002	0.11623	1.41360	0.05553	0.70353	8.74682	0.70338	0.00013
JUL 24 2014	Run68	200um/10Hz	MkAn1_61	0.00061	0.00000	0.00863	0.00003	0.16132	-0.00001	0.11618	1.41451	0.05608	0.70368	8.76833	0.70359	0.00015
JUL 25 2014	Run6	200um/10Hz	MkAn1_1	0.00073	0.00000	0.00926	0.00009	0.17127	-0.00001	0.12330	1.50077	0.05660	0.70349	8.76259	0.70345	0.00015
JUL 25 2014	Run7	200um/10Hz	MkAn1_2	0.00064	-0.00001	0.00825	0.00005	0.15199	0.00000	0.10938	1.33119	0.05683	0.70352	8.75837	0.70350	0.00017
JUL 25 2014	Run8	200um/10Hz	MkAn1_3	0.00073	-0.00002	0.00914	0.00005	0.16897	-0.00001	0.12162	1.48030	0.05667	0.70355	8.76053	0.70352	0.00010
JUL 25 2014	Run9	200um/10Hz	MkAn1_4	0.00079	-0.00002	0.00968	0.00002	0.17855	0.00000	0.12849	1.56437	0.05677	0.70344	8.76091	0.70341	0.00013
JUL 25 2014	Run10	200um/10Hz	MkAn1_5	0.00059	0.00000	0.00799	0.00004	0.14725	-0.00001	0.10595	1.28967	0.05684	0.70337	8.75807	0.70335	0.00014
JUL 26 2014	Run10	200um/10Hz	MkAn1_1	0.00054	0.00000	0.00635	0.00003	0.11686	-0.00001	0.08414	1.02456	0.05691	0.70354	8.76722	0.70353	0.00017
JUL 26 2014	Run11	200um/10Hz	MkAn1_2	0.00058	0.00001	0.00682	0.00017	0.12616	0.00000	0.09090	1.10618	0.05663	0.70353	8.76792	0.70349	0.00013
JUL 26 2014	Run12	200um/10Hz	MkAn1_3	0.00045	-0.00001	0.00559	0.00004	0.10370	0.00000	0.07467	0.90882	0.05648	0.70362	8.76379	0.70357	0.00022
JUL 26 2014	Run13	200um/10Hz	MkAn1_4	0.00046	-0.00001	0.00577	0.00012	0.10699	0.00000	0.07706	0.93788	0.05652	0.70343	8.76530	0.70338	0.00020
JUL 26 2014	Run14	200um/10Hz	MkAn1_5	0.00055	-0.00001	0.00672	0.00004	0.12461	-0.00001	0.08971	1.09240	0.05649	0.70344	8.76664	0.70339	0.00022
Average and error in 2SD													**0.70351**	**0.00021**	**0.70346**	**0.00017**
JUL 24 2014	Run13	100um/10Hz	MkAn1_6	0.00011	-0.00001	0.00212	0.00001	0.03820	-0.00002	0.02747	0.33436	0.05785	0.70347	8.75261	0.70355	0.00047
JUL 24 2014	Run14	100um/10Hz	MkAn1_7	0.00009	0.00000	0.00216	0.00001	0.03921	0.00000	0.02820	0.34328	0.05764	0.70335	8.75318	0.70341	0.00048
JUL 24 2014	Run15	100um/10Hz	MkAn1_8	0.00011	0.00000	0.00229	0.00001	0.04164	-0.00001	0.02996	0.36461	0.05761	0.70330	8.75377	0.70335	0.00047
JUL 24 2014	Run16	100um/10Hz	MkAn1_9	0.00012	-0.00001	0.00252	0.00001	0.04584	0.00001	0.03298	0.40156	0.05772	0.70343	8.75992	0.70349	0.00044
JUL 24 2014	Run17	100um/10Hz	MkAn1_10	0.00013	0.00001	0.00270	0.00002	0.04892	0.00000	0.03521	0.42854	0.05793	0.70337	8.75998	0.70346	0.00033
JUL 24 2014	Run43	100um/10Hz	MkAn1_36	0.00011	0.00000	0.00296	0.00003	0.05421	-0.00002	0.03899	0.47416	0.05703	0.70345	8.74680	0.70345	0.00024
JUL 24 2014	Run44	100um/10Hz	MkAn1_37	0.00009	0.00000	0.00297	0.00004	0.05595	0.00000	0.04025	0.48949	0.05553	0.70353	8.74905	0.70339	0.00029
JUL 24 2014	Run45	100um/10Hz	MkAn1_38	0.00009	-0.00001	0.00304	0.00004	0.05760	0.00000	0.04145	0.50413	0.05527	0.70354	8.75148	0.70337	0.00030
JUL 24 2014	Run46	100um/10Hz	MkAn1_39	0.00014	0.00000	0.00379	0.00003	0.07127	-0.00001	0.05127	0.62358	0.05560	0.70356	8.74834	0.70342	0.00025
JUL 24 2014	Run47	100um/10Hz	MkAn1_40	0.00011	-0.00001	0.00321	0.00003	0.06058	-0.00002	0.04356	0.52978	0.05533	0.70335	8.74575	0.70318	0.00027
Average and error in 2SD													**0.70343**	**0.00018**	**0.70341**	**0.00020**
JUL 24 2014	Run18	50um/10Hz	MkAn1_11	0.00006	-0.00002	0.00104	0.00000	0.01726	0.00000	0.01240	0.15087	0.06309	0.7031	8.7399	0.7037	0.0009
JUL 24 2014	Run19	50um/10Hz	MkAn1_12	0.00004	-0.00001	0.00091	0.00001	0.01684	0.00000	0.01212	0.14765	0.05659	0.7034	8.7675	0.7033	0.0007
JUL 24 2014	Run20	50um/10Hz	MkAn1_13	0.00005	0.00000	0.00091	0.00000	0.01576	0.00000	0.01134	0.13800	0.06021	0.7034	8.7545	0.7037	0.0007
JUL 24 2014	Run21	50um/10Hz	MkAn1_14	0.00006	-0.00001	0.00097	0.00000	0.01642	0.00000	0.01180	0.14364	0.06172	0.7033	8.7484	0.7038	0.0009
JUL 24 2014	Run22	50um/10Hz	MkAn1_15	0.00004	-0.00001	0.00088	0.00000	0.01575	-0.00002	0.01133	0.13789	0.05883	0.7034	8.7556	0.7036	0.0006
JUL 24 2014	Run23	50um/10Hz	MkAn1_16	0.00005	0.00000	0.00102	0.00000	0.01759	-0.00001	0.01263	0.15377	0.06061	0.7027	8.7427	0.7031	0.0007
JUL 24 2014	Run24	50um/10Hz	MkAn1_17	0.00005	0.00000	0.00096	0.00000	0.01651	-0.00001	0.01188	0.14448	0.06054	0.7038	8.7487	0.7041	0.0008
JUL 24 2014	Run25	50um/10Hz	MkAn1_18	0.00003	-0.00001	0.00091	0.00000	0.01614	-0.00002	0.01161	0.14117	0.05901	0.7040	8.7489	0.7042	0.0007
JUL 24 2014	Run26	50um/10Hz	MkAn1_19	0.00004	-0.00002	0.00090	0.00000	0.01594	-0.00001	0.01145	0.13936	0.05920	0.7031	8.7429	0.7033	0.0008
JUL 24 2014	Run27	50um/10Hz	MkAn1_20	0.00005	-0.00002	0.00089	0.00001	0.01567	-0.00002	0.01127	0.13716	0.05951	0.7031	8.7512	0.7033	0.0008
JUL 24 2014	Run28	50um/10Hz	MkAn1_21	0.00004	0.00001	0.00094	0.00001	0.01662	-0.00001	0.01196	0.14547	0.05954	0.7037	8.7549	0.7040	0.0006
JUL 24 2014	Run29	50um/10Hz	MkAn1_22	0.00003	-0.00001	0.00100	0.00001	0.01784	-0.00001	0.01285	0.15618	0.05895	0.7043	8.7549	0.7045	0.0008
JUL 24 2014	Run30	50um/10Hz	MkAn1_23	0.00004	-0.00001	0.00101	0.00000	0.01778	-0.00002	0.01280	0.15572	0.05947	0.7039	8.7580	0.7041	0.0008
JUL 24 2014	Run31	50um/10Hz	MkAn1_24	0.00004	0.00000	0.00100	0.00000	0.01786	-0.00001	0.01285	0.15646	0.05889	0.7032	8.7572	0.7033	0.0006
JUL 24 2014	Run32	50um/10Hz	MkAn1_25	0.00004	-0.00002	0.00103	0.00000	0.01827	-0.00001	0.01314	0.15986	0.05915	0.7037	8.7513	0.7039	0.0007
JUL 24 2014	Run33	50um/10Hz	MkAn1_26	0.00005	-0.00001	0.00101	0.00000	0.01797	0.00000	0.01293	0.15727	0.05857	0.7041	8.7532	0.7042	0.0007
JUL 24 2014	Run34	50um/10Hz	MkAn1_27	0.00005	-0.00002	0.00103	0.00001	0.01815	0.00000	0.01306	0.15886	0.05944	0.7033	8.7507	0.7035	0.0008
JUL 24 2014	Run35	50um/10Hz	MkAn1_28	0.00005	-0.00001	0.00101	-0.00001	0.01812	0.00000	0.01303	0.15859	0.05855	0.7033	8.7516	0.7034	0.0006
JUL 24 2014	Run36	50um/10Hz	MkAn1_29	0.00004	0.00000	0.00097	0.00002	0.01737	-0.00001	0.01249	0.15195	0.05828	0.7031	8.7489	0.7032	0.0009
JUL 24 2014	Run37	50um/10Hz	MkAn1_30	0.00004	-0.00001	0.00100	0.00001	0.01779	-0.00002	0.01279	0.15563	0.05903	0.7029	8.7466	0.7031	0.0007
JUL 24 2014	Run48	50um/10Hz	MkAn1_41	0.00000	-0.00001	0.00078	0.00003	0.01530	-0.00002	0.01102	0.13388	0.05360	0.7036	8.7495	0.7033	0.0009
JUL 24 2014	Run49	50um/10Hz	MkAn1_42	0.00002	0.00000	0.00089	0.00001	0.01691	-0.00001	0.01217	0.14794	0.05506	0.7039	8.7481	0.7037	0.0008
JUL 24 2014	Run50	50um/10Hz	MkAn1_43	0.00002	-0.00002	0.00096	0.00001	0.01818	0.00001	0.01308	0.15913	0.05537	0.7031	8.7497	0.7030	0.0007
JUL 24 2014	Run51	50um/10Hz	MkAn1_44	0.00002	0.00001	0.00098	0.00001	0.01843	-0.00001	0.01327	0.16140	0.05557	0.7040	8.7574	0.7039	0.0008
JUL 24 2014	Run52	50um/10Hz	MkAn1_45	0.00002	-0.00002	0.00099	0.00001	0.01886	-0.00001	0.01356	0.16514	0.05499	0.7029	8.7546	0.7027	0.0009
JUL 24 2014	Run53	50um/10Hz	MkAn1_46	0.00002	0.00000	0.00097	0.00001	0.01824	-0.00001	0.01313	0.15971	0.05581	0.7036	8.7519	0.7035	0.0007
JUL 24 2014	Run54	50um/10Hz	MkAn1_47	0.00002	-0.00001	0.00095	0.00000	0.01798	-0.00001	0.01293	0.15739	0.05536	0.7033	8.7505	0.7031	0.0007
JUL 24 2014	Run55	50um/10Hz	MkAn1_48	0.00002	-0.00002	0.00090	0.00001	0.01722	-0.00001	0.01239	0.15079	0.05475	0.7036	8.7565	0.7034	0.0008
JUL 24 2014	Run56	50um/10Hz	MkAn1_49	0.00002	-0.00002	0.00092	0.00000	0.01768	0.00000	0.01273	0.15472	0.05415	0.7042	8.7505	0.7040	0.0006
JUL 24 2014	Run57	50um/10Hz	MkAn1_50	0.00003	-0.00001	0.00101	0.00000	0.01872	0.00000	0.01347	0.16387	0.05633	0.7036	8.7505	0.7035	0.0007
JUL 24 2014	Run58	50um/10Hz	MkAn1_51	0.00002	-0.00001	0.00100	0.00000	0.01887	0.00000	0.01357	0.16513	0.05506	0.7034	8.7420	0.7032	0.0009
JUL 24 2014	Run59	50um/10Hz	MkAn1_52	0.00003	0.00000	0.00089	0.00000	0.01727	-0.00001	0.01244	0.15128	0.05408	0.7042	8.7545	0.7039	0.0008
JUL 24 2014	Run60	50um/10Hz	MkAn1_53	0.00002	0.00000	0.00095	0.00000	0.01798	-0.00002	0.01293	0.15735	0.05533	0.7032	8.7465	0.7031	0.0007
JUL 24 2014	Run61	50um/10Hz	MkAn1_54	0.00001	-0.00001	0.00098	0.00002	0.01856	-0.00001	0.01336	0.16247	0.05550	0.7038	8.7513	0.7036	0.0006
JUL 24 2014	Run62	50um/10Hz	MkAn1_55	0.00002	-0.00001	0.00099	0.00000	0.01868	0.00000	0.01344	0.16348	0.05563	0.7036	8.7484	0.7035	0.0007
JUL 24 2014	Run63	50um/10Hz	MkAn1_56	0.00002	0.00001	0.00097	0.00003	0.01825	-0.00001	0.01313	0.15972	0.05558	0.7033	8.7506	0.7032	0.0007
JUL 24 2014	Run64	50um/10Hz	MkAn1_57	0.00003	0.00000	0.00097	0.00004	0.01824	0.00000	0.01314	0.15972	0.05538	0.7036	8.7530	0.7034	0.0006
JUL 24 2014	Run65	50um/10Hz	MkAn1_58	0.00003	0.00000	0.00098	0.00001	0.01823	-0.00001	0.01311	0.15938	0.05617	0.7036	8.7383	0.7035	0.0005
JUL 24 2014	Run66	50um/10Hz	MkAn1_59	0.00000	0.00000	0.00099	0.00001	0.01876	-0.00001	0.01352	0.16424	0.05492	0.7043	8.7499	0.7041	0.0007
JUL 24 2014	Run67	50um/10Hz	MkAn1_60	0.00002	0.00000	0.00099	0.00001	0.01853	0.00000	0.01333	0.16208	0.05567	0.7038	8.7469	0.7037	0.0009
Average and error in 2SD													**0.7035**	**0.0008**	**0.7036**	**0.0008**

Day	Run ID	Crater	Sample	^{83}Kr (V)	$^{83.5}$M (V)	^{84}Sr (V)	^{85}Rb (V)	^{86}Sr (V)	$^{86.5}$M (V)	^{87}Sr (V)	^{88}Sr (V)	^{84}Sr/^{86}Sr	^{87}Sr/^{86}Sr	^{88}Sr/^{86}Sr	^{87}Sr/^{86}Sr cor	2SE
JUL 25 2014	Run11	200um/10Hz	BHVO-2G_1	0.00031	0.00005	0.01281	0.08395	0.23632	0.00001	0.20411	2.07189	0.05678	0.70341	8.76719	0.70334	0.00013
JUL 25 2014	Run12	200um/10Hz	BHVO-2G_2	0.00033	0.00006	0.01399	0.08743	0.25980	0.00001	0.22241	2.27714	0.05642	0.70349	8.76492	0.70338	0.00012
JUL 25 2014	Run13	200um/10Hz	BHVO-2G_3	0.00031	0.00006	0.01332	0.08799	0.24680	0.00001	0.21327	2.16323	0.05653	0.70341	8.76501	0.70331	0.00014
JUL 25 2014	Run14	200um/10Hz	BHVO-2G_4	0.00030	0.00006	0.01308	0.08851	0.24303	0.00002	0.21074	2.13006	0.05637	0.70336	8.76474	0.70325	0.00016
JUL 25 2014	Run15	200um/10Hz	BHVO-2G_5	0.00030	0.00006	0.01284	0.08909	0.23823	0.00001	0.20752	2.08746	0.05644	0.70343	8.76245	0.70332	0.00013
JUL 26 2014	Run15	200um/10Hz	BHVO-2G_1	0.00028	0.00004	0.01092	0.08020	0.20259	0.00000	0.17839	1.77733	0.05653	0.70344	8.77301	0.70339	0.00015
JUL 26 2014	Run16	200um/10Hz	BHVO-2G_2	0.00029	0.00006	0.01096	0.08266	0.20340	0.00001	0.17995	1.78418	0.05649	0.70343	8.77159	0.70338	0.00020
JUL 26 2014	Run17	200um/10Hz	BHVO-2G_3	0.00026	0.00005	0.01066	0.08156	0.19868	0.00002	0.17612	1.74249	0.05623	0.70353	8.77007	0.70345	0.00020
JUL 26 2014	Run18	200um/10Hz	BHVO-2G_4	0.00026	0.00005	0.01073	0.08302	0.19976	0.00001	0.17746	1.75166	0.05630	0.70347	8.76887	0.70340	0.00016
JUL 26 2014	Run19	200um/10Hz	BHVO-2G_5	0.00029	0.00005	0.01167	0.08546	0.21771	0.00002	0.19140	1.90963	0.05622	0.70350	8.77138	0.70342	0.00023
JUN 02 2014	Run16	100um/10Hz	BHVO-2G-1	0.00018	0.00002	0.00691	0.03122	0.12686	0.00001	0.10395	1.11127	0.05691	0.70354	8.74310	0.70354	0.00019
JUN 02 2014	Run17	100um/10Hz	BHVO-2G-2	0.00018	0.00002	0.00750	0.03473	0.13870	0.00001	0.11392	1.21623	0.05665	0.70342	8.76855	0.70342	0.00018
JUN 02 2014	Run18	100um/10Hz	BHVO-2G-3	0.00018	0.00002	0.00768	0.03535	0.14254	0.00000	0.11697	1.25006	0.05647	0.70366	8.76957	0.70366	0.00016
JUN 02 2014	Run19	100um/10Hz	BHVO-2G-4	0.00017	0.00002	0.00766	0.03488	0.14200	-0.00001	0.11636	1.24483	0.05651	0.70358	8.76609	0.70358	0.00014
JUN 02 2014	Run20	100um/10Hz	BHVO-2G-5	0.00018	0.00002	0.00769	0.03543	0.14257	0.00000	0.11699	1.24981	0.05651	0.70360	8.76603	0.70360	0.00018
JUN 02 2014	Run22	100um/10Hz	BHVO-2G-6	0.00019	0.00002	0.00765	0.03442	0.14124	-0.00001	0.11559	1.23807	0.05673	0.70342	8.76559	0.70342	0.00015
JUN 02 2014	Run23	100um/10Hz	BHVO-2G-7	0.00018	0.00002	0.00771	0.03511	0.14287	0.00000	0.11706	1.25231	0.05655	0.70352	8.76541	0.70352	0.00016
JUN 02 2014	Run243	100um/10Hz	BHVO-2G-8	0.00017	0.00002	0.00759	0.03479	0.14052	0.00001	0.11524	1.23166	0.05656	0.70354	8.76497	0.70354	0.00016
JUN 02 2014	Run25	100um/10Hz	BHVO-2G-9	0.00017	0.00002	0.00744	0.03455	0.13786	0.00000	0.11324	1.20842	0.05657	0.70359	8.76534	0.70359	0.00016
JUN 02 2014	Run26	100um/10Hz	BHVO-2G-10	0.00017	0.00003	0.00735	0.03391	0.13615	0.00000	0.11172	1.19333	0.05660	0.70344	8.76486	0.70344	0.00020
JUN 02 2014	Run28	100um/10Hz	BHVO-2G-11	0.00017	0.00002	0.00737	0.03549	0.13631	0.00000	0.11247	1.19494	0.05669	0.70337	8.76617	0.70337	0.00019
JUN 02 2014	Run29	100um/10Hz	BHVO-2G-12	0.00018	0.00003	0.00742	0.03502	0.13729	0.00001	0.11301	1.20359	0.05661	0.70347	8.76685	0.70347	0.00015
JUN 02 2014	Run30	100um/10Hz	BHVO-2G-13	0.00014	0.00001	0.00685	0.03457	0.12700	0.00000	0.10542	1.11332	0.05656	0.70347	8.76637	0.70347	0.00019
JUN 02 2014	Run31	100um/10Hz	BHVO-2G-14	0.00016	0.00002	0.00735	0.03415	0.13617	0.00000	0.11185	1.19391	0.05656	0.70343	8.76733	0.70343	0.00018
JUN 02 2014	Run32	100um/10Hz	BHVO-2G-15	0.00015	0.00001	0.00699	0.03309	0.12951	0.00000	0.10664	1.13536	0.05658	0.70352	8.76645	0.70352	0.00019
Average and error in 2SD													**0.70348**	**0.00015**	**0.70345**	**0.00020**
JUL 25 2014	Run22	50um/10Hz	BHVO-2G_1	0.00004	-0.00002	0.00170	0.00991	0.03084	0.00000	0.02621	0.27031	0.05799	0.7034	8.7643	0.7035	0.0005

JUL 25 2014	Run23	50um/10Hz	BHVO-2G_2	0.00004	0.00001	0.00171	0.01014	0.03137	-0.00001	0.02670	0.27526	0.05729	0.7037	8.7731	0.7036	0.0004
JUL 25 2014	Run24	50um/10Hz	BHVO-2G_3	0.00003	0.00000	0.00177	0.01046	0.03214	0.00000	0.02737	0.28173	0.05776	0.7034	8.7655	0.7034	0.0005
JUL 25 2014	Run25	50um/10Hz	BHVO-2G_4	0.00004	0.00000	0.00183	0.01097	0.03313	0.00000	0.02829	0.29048	0.05799	0.7035	8.7658	0.7036	0.0005
JUL 25 2014	Run26	50um/10Hz	BHVO-2G_5	0.00004	0.00001	0.00180	0.01112	0.03335	0.00001	0.02851	0.29244	0.05666	0.7033	8.7664	0.7032	0.0004
JUL 25 2014	Run27	50um/10Hz	BHVO-2G_6	0.00004	0.00000	0.00180	0.01109	0.03319	-0.00001	0.02839	0.29111	0.05698	0.7035	8.7684	0.7034	0.0004
JUL 25 2014	Run28	50um/10Hz	BHVO-2G_7	0.00004	0.00000	0.00182	0.01108	0.03305	-0.00001	0.02828	0.28988	0.05758	0.7034	8.7694	0.7034	0.0005
JUL 25 2014	Run29	50um/10Hz	BHVO-2G_8	0.00004	-0.00001	0.00184	0.01137	0.03399	0.00000	0.02906	0.29807	0.05669	0.7029	8.7679	0.7028	0.0005
JUL 25 2014	Run30	50um/10Hz	BHVO-2G_9	0.00002	0.00000	0.00189	0.01144	0.03454	0.00000	0.02950	0.30276	0.05722	0.7036	8.7625	0.7036	0.0005
JUL 25 2014	Run31	50um/10Hz	BHVO-2G_10	0.00003	0.00001	0.00191	0.01156	0.03542	0.00000	0.03017	0.31038	0.05662	0.7035	8.7620	0.7034	0.0004
JUL 25 2014	Run32	50um/10Hz	BHVO-2G_11	0.00004	0.00002	0.00200	0.01189	0.03654	-0.00002	0.03112	0.32023	0.05731	0.7036	8.7641	0.7036	0.0005
JUL 25 2014	Run33	50um/10Hz	BHVO-2G_12	0.00005	0.00002	0.00201	0.01185	0.03657	0.00001	0.03112	0.32060	0.05774	0.7035	8.7671	0.7035	0.0005
JUL 25 2014	Run34	50um/10Hz	BHVO-2G_13	0.00003	0.00001	0.00197	0.01177	0.03623	0.00000	0.03085	0.31748	0.05699	0.7036	8.7638	0.7036	0.0005
JUL 25 2014	Run35	50um/10Hz	BHVO-2G_14	0.00004	0.00000	0.00197	0.01176	0.03625	0.00000	0.03086	0.31772	0.05682	0.7037	8.7644	0.7036	0.0005
JUL 25 2014	Run36	50um/10Hz	BHVO-2G_15	0.00002	0.00001	0.00193	0.01140	0.03568	0.00000	0.03028	0.31249	0.05656	0.7031	8.7587	0.7030	0.0005
JUL 25 2014	Run37	50um/10Hz	BHVO-2G_16	0.00005	0.00001	0.00197	0.01179	0.03625	0.00001	0.03086	0.31754	0.05706	0.7035	8.7619	0.7034	0.0006
JUL 25 2014	Run38	50um/10Hz	BHVO-2G_17	0.00004	0.00000	0.00197	0.01202	0.03647	-0.00001	0.03113	0.31954	0.05670	0.7040	8.7627	0.7039	0.0005
JUL 25 2014	Run39	50um/10Hz	BHVO-2G_18	0.00004	0.00001	0.00198	0.01199	0.03616	0.00000	0.03090	0.31694	0.05736	0.7039	8.7637	0.7039	0.0005
JUL 25 2014	Run40	50um/10Hz	BHVO-2G_19	0.00004	0.00000	0.00198	0.01213	0.03649	-0.00001	0.03117	0.31983	0.05693	0.7033	8.7641	0.7033	0.0006
JUL 25 2014	Run41	50um/10Hz	BHVO-2G_20	0.00004	0.00002	0.00196	0.01230	0.03630	0.00001	0.03112	0.31829	0.05657	0.7035	8.7669	0.7034	0.0005
JUL 26 2014	Run20	50um/10Hz	BHVO-2G_1	0.00004	0.00001	0.00173	0.01025	0.03169	-0.00001	0.02698	0.27806	0.05718	0.7036	8.7748	0.7036	0.0005
JUL 26 2014	Run21	50um/10Hz	BHVO-2G_2	0.00001	0.00002	0.00164	0.01011	0.03011	-0.00001	0.02576	0.26406	0.05721	0.7031	8.7688	0.7031	0.0006
JUL 26 2014	Run22	50um/10Hz	BHVO-2G_3	0.00003	-0.00001	0.00168	0.01031	0.03109	0.00000	0.02655	0.27264	0.05665	0.7032	8.7696	0.7032	0.0006
JUL 26 2014	Run23	50um/10Hz	BHVO-2G_4	0.00006	0.00001	0.00165	0.00976	0.03003	0.00001	0.02557	0.26335	0.05751	0.7032	8.7687	0.7033	0.0006
JUL 26 2014	Run24	50um/10Hz	BHVO-2G_5	0.00003	0.00000	0.00180	0.01007	0.03274	-0.00001	0.02766	0.28722	0.05756	0.7035	8.7724	0.7036	0.0005
JUL 26 2014	Run25	50um/10Hz	BHVO-2G_6	0.00004	0.00001	0.00185	0.01124	0.03389	0.00000	0.02895	0.29703	0.05724	0.7036	8.7641	0.7036	0.0006
JUL 26 2014	Run26	50um/10Hz	BHVO-2G_7	0.00005	0.00001	0.00181	0.01091	0.03292	0.00000	0.02813	0.28872	0.05779	0.7035	8.7687	0.7036	0.0005
JUL 26 2014	Run27	50um/10Hz	BHVO-2G_8	0.00004	0.00000	0.00177	0.01066	0.03255	0.00000	0.02776	0.28540	0.05701	0.7038	8.7692	0.7038	0.0005
JUL 26 2014	Run28	50um/10Hz	BHVO-2G_9	0.00005	0.00000	0.00180	0.01056	0.03273	0.00000	0.02784	0.28679	0.05747	0.7037	8.7635	0.7037	0.0005
JUL 26 2014	Run29	50um/10Hz	BHVO-2G_10	0.00004	0.00001	0.00174	0.01059	0.03213	-0.00001	0.02742	0.28170	0.05679	0.7033	8.7666	0.7033	0.0004
JUL 26 2014	Run30	50um/10Hz	BHVO-2G_11	0.00003	0.00000	0.00169	0.01040	0.03132	0.00000	0.02675	0.27462	0.05658	0.7031	8.7678	0.7031	0.0006
JUL 26 2014	Run31	50um/10Hz	BHVO-2G_12	0.00003	-0.00001	0.00176	0.01090	0.03241	-0.00001	0.02776	0.28429	0.05711	0.7037	8.7721	0.7037	0.0004
JUL 26 2014	Run32	50um/10Hz	BHVO-2G_13	0.00003	0.00002	0.00166	0.00975	0.03039	-0.00001	0.02585	0.26669	0.05744	0.7039	8.7747	0.7040	0.0006
JUL 26 2014	Run33	50um/10Hz	BHVO-2G_14	0.00002	0.00000	0.00160	0.00968	0.02946	0.00001	0.02514	0.25853	0.05689	0.7035	8.7743	0.7035	0.0005
JUL 26 2014	Run34	50um/10Hz	BHVO-2G_15	0.00005	0.00000	0.00157	0.00939	0.02855	0.00001	0.02436	0.25047	0.05750	0.7033	8.7700	0.7033	0.0007
JUL 26 2014	Run35	50um/10Hz	BHVO-2G_16	0.00003	0.00000	0.00172	0.01003	0.03178	-0.00002	0.02694	0.27893	0.05692	0.7032	8.7762	0.7032	0.0004
JUL 26 2014	Run36	50um/10Hz	BHVO-2G_17	0.00004	0.00001	0.00169	0.00988	0.03129	-0.00002	0.02654	0.27470	0.05663	0.7033	8.7765	0.7032	0.0005
JUL 26 2014	Run37	50um/10Hz	BHVO-2G_18	0.00005	0.00001	0.00161	0.00980	0.02958	0.00000	0.02528	0.25952	0.05689	0.7036	8.7734	0.7036	0.0006
JUL 26 2014	Run38	50um/10Hz	BHVO-2G_19	0.00002	-0.00001	0.00160	0.00956	0.02947	-0.00001	0.02510	0.25849	0.05685	0.7036	8.7706	0.7036	0.0007
JUL 26 2014	Run39	50um/10Hz	BHVO-2G_20	0.00002	0.00001	0.00160	0.00965	0.02963	0.00000	0.02525	0.25983	0.05653	0.7038	8.7679	0.7037	0.0005
JUN 02 2014	Run34	50um/10Hz	BHVO-2G-16	0.00005	0.00002	0.00214	0.01045	0.03911	0.00000	0.03238	0.34279	0.05733	0.7035	8.7642	0.7035	0.0004
JUN 02 2014	Run35	50um/10Hz	BHVO-2G-17	0.00005	0.00000	0.00203	0.00994	0.03753	0.00000	0.03104	0.32896	0.05666	0.7036	8.7644	0.7036	0.0005
JUN 02 2014	Run36	50um/10Hz	BHVO-2G-18	0.00004	-0.00001	0.00201	0.00995	0.03722	-0.00002	0.03082	0.32640	0.05673	0.7033	8.7696	0.7033	0.0004
JUN 02 2014	Run37	50um/10Hz	BHVO-2G-19	0.00004	0.00000	0.00199	0.01002	0.03672	-0.00001	0.03048	0.32183	0.05667	0.7032	8.7640	0.7032	0.0004
JUN 02 2014	Run38	50um/10Hz	BHVO-2G-20	0.00003	0.00000	0.00199	0.00998	0.03663	-0.00001	0.03041	0.32103	0.05701	0.7037	8.7653	0.7037	0.0005
JUN 02 2014	Run40	50um/10Hz	BHVO-2G-21	0.00003	0.00002	0.00212	0.01025	0.03865	0.00000	0.03198	0.33874	0.05744	0.7036	8.7631	0.7036	0.0004
JUN 02 2014	Run41	50um/10Hz	BHVO-2G-22	0.00005	0.00001	0.00202	0.01004	0.03731	0.00000	0.03092	0.32705	0.05676	0.7034	8.7656	0.7034	0.0004
JUN 02 2014	Run42	50um/10Hz	BHVO-2G-23	0.00005	0.00001	0.00203	0.01021	0.03748	-0.00001	0.03111	0.32852	0.05679	0.7035	8.7654	0.7035	0.0004
JUN 02 2014	Run43	50um/10Hz	BHVO-2G-24	0.00005	0.00002	0.00203	0.01025	0.03765	0.00001	0.03126	0.33002	0.05658	0.7035	8.7647	0.7035	0.0004
JUN 02 2014	Run44	50um/10Hz	BHVO-2G-25	0.00004	0.00000	0.00210	0.01045	0.03884	0.00000	0.03219	0.34030	0.05672	0.7038	8.7624	0.7038	0.0003
JUN 02 2014	Run46	50um/10Hz	BHVO-2G-26	0.00003	-0.00001	0.00195	0.00972	0.03563	-0.00001	0.02958	0.31218	0.05733	0.7037	8.7612	0.7037	0.0005
JUN 02 2014	Run47	50um/10Hz	BHVO-2G-27	0.00004	0.00001	0.00199	0.00973	0.03636	0.00000	0.03013	0.31883	0.05724	0.7037	8.7693	0.7037	0.0005
JUN 02 2014	Run48	50um/10Hz	BHVO-2G-28	0.00004	0.00001	0.00210	0.01009	0.03880	0.00000	0.03202	0.34012	0.05673	0.7035	8.7656	0.7035	0.0004
JUN 02 2014	Run49	50um/10Hz	BHVO-2G-29	0.00005	0.00000	0.00217	0.01042	0.03996	-0.00001	0.03299	0.35036	0.05685	0.7035	8.7679	0.7035	0.0004
JUN 02 2014	Run50	50um/10Hz	BHVO-2G-30	0.00004	0.00000	0.00195	0.00989	0.03595	0.00000	0.02988	0.31518	0.05688	0.7032	8.7685	0.7032	0.0005
Average and error in 2SD													**0.7035**	**0.0004**	**0.7035**	**0.0005**

Day	Run ID	Crater	Sample	^{83}Kr (V)	$^{83.5}$M (V)	^{84}Sr (V)	^{85}Rb (V)	^{86}Sr (V)	$^{86.5}$M (V)	^{87}Sr (V)	^{88}Sr (V)	^{84}Sr/^{86}Sr	^{87}Sr/^{86}Sr	^{88}Sr/^{86}Sr	^{87}Sr/^{86}Sr cor	2SE
JUL 27 2014	Run2	100um/10Hz	BCR-2G_1	0.00014	0.00003	0.00432	0.13576	0.08026	-0.00001	0.11296	0.70442	0.05648	0.70488	8.77626	0.70488	0.00052
JUL 27 2014	Run3	100um/10Hz	BCR-2G_2	0.00017	0.00003	0.00433	0.13609	0.07974	0.00002	0.11274	0.69979	0.05694	0.70523	8.77537	0.70524	0.00039
JUL 27 2014	Run4	100um/10Hz	BCR-2G_3	0.00015	0.00005	0.00432	0.13606	0.07953	0.00001	0.11257	0.69792	0.05702	0.70512	8.77507	0.70513	0.00042
JUL 27 2014	Run5	100um/10Hz	BCR-2G_4	0.00016	0.00003	0.00436	0.13599	0.08056	-0.00001	0.11327	0.70693	0.05678	0.70472	8.77516	0.70497	0.00049
JUL 27 2014	Run7	100um/10Hz	BCR-2G_6	0.00014	0.00002	0.00441	0.13720	0.08090	0.00001	0.11397	0.70981	0.05719	0.70467	8.77392	0.70498	0.00036
JUL 27 2014	Run8	100um/10Hz	BCR-2G_7	0.00015	0.00002	0.00449	0.13659	0.08272	0.00001	0.11503	0.72557	0.05690	0.70464	8.77185	0.70469	0.00036
JUL 27 2014	Run9	100um/10Hz	BCR-2G_8	0.00015	0.00002	0.00450	0.14468	0.08278	0.00000	0.11837	0.72613	0.05693	0.70480	8.77124	0.70467	0.00055
JUL 27 2014	Run10	100um/10Hz	BCR-2G_9	0.00014	0.00004	0.00468	0.14763	0.08640	0.00002	0.12219	0.75783	0.05679	0.70498	8.77120	0.70484	0.00037
JUL 27 2014	Run11	100um/10Hz	BCR-2G_10	0.00015	0.00004	0.00482	0.15370	0.08903	0.00001	0.12653	0.78103	0.05671	0.70476	8.77238	0.70501	0.00039
JUL 27 2014	Run13	100um/10Hz	BCR-2G_11	0.00018	0.00002	0.00485	0.16231	0.08926	0.00001	0.13020	0.78260	0.05695	0.70512	8.76735	0.70480	0.00071
JUL 27 2014	Run14	100um/10Hz	BCR-2G_12	0.00015	0.00003	0.00484	0.16377	0.08944	0.00001	0.13090	0.78423	0.05674	0.70486	8.76885	0.70519	0.00040
JUL 27 2014	Run15	100um/10Hz	BCR-2G_13	0.00015	0.00003	0.00479	0.16148	0.08842	0.00002	0.12922	0.77527	0.05677	0.70468	8.76767	0.70496	0.00047
JUL 27 2014	Run16	100um/10Hz	BCR-2G_14	0.00015	0.00004	0.00473	0.16152	0.08757	0.00001	0.12863	0.76814	0.05665	0.70469	8.77158	0.70478	0.00042
JUL 27 2014	Run17	100um/10Hz	BCR-2G_15	0.00015	0.00004	0.00471	0.15223	0.08698	0.00000	0.12443	0.76317	0.05683	0.70451	8.77388	0.70482	0.00045
JUL 27 2014	Run19	100um/10Hz	BCR-2G_16	0.00016	0.00003	0.00474	0.15804	0.08706	0.00001	0.12685	0.76355	0.05702	0.70489	8.76999	0.70469	0.00050
JUL 27 2014	Run20	100um/10Hz	BCR-2G_17	0.00014	0.00003	0.00469	0.15062	0.08648	0.00001	0.12342	0.75847	0.05682	0.70492	8.77002	0.70491	0.00043
JUL 27 2014	Run21	100um/10Hz	BCR-2G_18	0.00014	0.00004	0.00481	0.15730	0.08893	0.00002	0.12789	0.77993	0.05664	0.70478	8.76947	0.70494	0.00044
JUL 27 2014	Run22	100um/10Hz	BCR-2G_19	0.00014	0.00002	0.00456	0.15067	0.08419	0.00000	0.12176	0.73841	0.05673	0.70450	8.77042	0.70485	0.00036
JUL 27 2014	Run23	100um/10Hz	BCR-2G_20	0.00014	0.00003	0.00434	0.14427	0.08001	0.00001	0.11615	0.70182	0.05684	0.70437	8.77120	0.70459	0.00043
JUL 27 2014	Run25	100um/10Hz	BCR-2G_20	0.00014	0.00002	0.00433	0.14613	0.07952	0.00001	0.11654	0.69714	0.05707	0.70465	8.76628	0.70450	0.00046
JUL 27 2014	Run26	100um/10Hz	BCR-2G_21	0.00013	0.00004	0.00457	0.14750	0.08428	0.00001	0.12056	0.73905	0.05680	0.70487	8.76861	0.70470	0.00039
JUL 27 2014	Run27	100um/10Hz	BCR-2G_22	0.00016	0.00004	0.00479	0.14845	0.08870	0.00000	0.12412	0.77763	0.05660	0.70484	8.76674	0.70499	0.00030
JUL 27 2014	Run28	100um/10Hz	BCR-2G_23	0.00014	0.00003	0.00490	0.15379	0.09040	0.00001	0.12748	0.79235	0.05685	0.70470	8.76522	0.70502	0.00048
JUL 27 2014	Run29	100um/10Hz	BCR-2G_24	0.00016	0.00005	0.00497	0.15569	0.09163	0.00002	0.12915	0.80323	0.05686	0.70471	8.76605	0.70493	0.00048
JUL 27 2014	Run32	100um/10Hz	BCR-2G_25	0.00017	0.00003	0.00479	0.15387	0.08783	0.00002	0.12567	0.76993	0.05715	0.70477	8.76564	0.70500	0.00059
JUL 27 2014	Run33	100um/10Hz	BCR-2G_26	0.00015	0.00002	0.00470	0.15413	0.08681	0.00001	0.12505	0.76101	0.05667	0.70487	8.76606	0.70503	0.00044
JUL 27 2014	Run34	100um/10Hz	BCR-2G_27	0.00015	0.00004	0.00479	0.15653	0.08823	0.00001	0.12702	0.77336	0.05691	0.70465	8.76547	0.70521	0.00047
JUL 27 2014	Run35	100um/10Hz	BCR-2G_28	0.00015	0.00002	0.00511	0.16211	0.09432	0.00001	0.13366	0.82650	0.05675	0.70467	8.76219	0.70502	0.00053
JUL 27 2014	Run36	100um/10Hz	BCR-2G_29	0.00014	0.00002	0.00495	0.15888	0.09123	0.00002	0.13010	0.79909	0.05675	0.70451	8.75889	0.70508	0.00041
JUL 27 2014	Run38	100um/10Hz	BCR-2G_30	0.00015	0.00003	0.00478	0.14790	0.08809	0.00001	0.12342	0.77217	0.05693	0.70500	8.76570	0.70501	0.00055
JUL 27 2014	Run39	100um/10Hz	BCR-2G_31	0.00015	0.00002	0.00488	0.14975	0.08994	0.00000	0.12551	0.78829	0.05682	0.70501	8.76404	0.70519	0.00042
JUL 27 2014	Run40	100um/10Hz	BCR-2G_32	0.00014	0.00002	0.00504	0.15470	0.09298	0.00001	0.12970	0.81479	0.05684	0.70504	8.76317	0.70521	0.00042
JUL 27 2014	Run41	100um/10Hz	BCR-2G_33	0.00014	0.00003	0.00519	0.15843	0.09592	0.00000	0.13333	0.84036	0.05663	0.70509	8.76082	0.70525	0.00060
JUL 27 2014	Run42	100um/10Hz	BCR-2G_34	0.00015	0.00003	0.00522	0.15885	0.09660	0.00001	0.13400	0.84647	0.05655	0.70510	8.76208	0.70530	0.00046
JUL 27 2014	Run45	100um/10Hz	BCR-2G_35	0.00015	0.00003	0.00519	0.15108	0.09509	0.00001	0.12973	0.83301	0.05716	0.70475	8.76038	0.70532	0.00042
JUL 27 2014	Run46	100um/10Hz	BCR-2G_36	0.00014	0.00002	0.00493	0.14730	0.09104	0.00002	0.12532	0.79792	0.05668	0.70496	8.76439	0.70473	0.00044
JUL 27 2014	Run47	100um/10Hz	BCR-2G_37	0.00014	0.00003	0.00474	0.15163	0.08751	-0.00002	0.12451	0.76691	0.05671	0.70484	8.76362	0.70494	0.00043
JUL 27 2014	Run48	100um/10Hz	BCR-2G_38	0.00015	0.00003	0.00458	0.14789	0.08453	0.00000	0.12086	0.74097	0.05675	0.70485	8.76559	0.70481	0.00043
JUL 27 2014	Run49	100um/10Hz	BCR-2G_39	0.00015	0.00003	0.00450	0.14565	0.08336	0.00001	0.11912	0.73060	0.05661	0.70513	8.76420	0.70483	0.00035
Average and error in 2SD													**0.70482**	**0.00040**	**0.70495**	**0.00040**
JUL 27 2014	Run51	50um/10Hz	BCR-2G_40	0.00005	0.00001	0.00124	0.03832	0.02253	0.00001	0.03177	0.19751	0.05779	0.7050	8.7675	0.7050	0.0008
JUL 27 2014	Run52	50um/10Hz	BCR-2G_41	0.00003	-0.00001	0.00122	0.03799	0.02226	-0.00001	0.03145	0.19526	0.05765	0.7052	8.7717	0.7052	0.0009
JUL 27 2014	Run53	50um/10Hz	BCR-2G_42	0.00003	0.00000	0.00119	0.03741	0.02165	-0.00001	0.03077	0.18986	0.05740	0.7048	8.7688	0.7048	0.0009
JUL 27 2014	Run54	50um/10Hz	BCR-2G_43	0.00003	0.00001	0.00114	0.03621	0.02095	-0.00001	0.02979	0.18354	0.05696	0.7056	8.7606	0.7056	0.0009
JUL 27 2014	Run55	50um/10Hz	BCR-2G_44	0.00003	-0.00002	0.00116	0.03678	0.02122	0.00000	0.03020	0.18604	0.05727	0.7051	8.7679	0.7051	0.0010
JUL 27 2014	Run56	50um/10Hz	BCR-2G_45	0.00002	0.00000	0.00121	0.03815	0.02228	0.00000	0.03152	0.19538	0.05703	0.7048	8.7682	0.7049	0.0008
JUL 27 2014	Run57	50um/10Hz	BCR-2G_46	0.00004	0.00000	0.00120	0.03830	0.02213	0.00001	0.03148	0.19395	0.05684	0.7052	8.7627	0.7054	0.0009
JUL 27 2014	Run58	50um/10Hz	BCR-2G_47	0.00002	0.00001	0.00113	0.03583	0.02089	-0.00001	0.02958	0.18307	0.05647	0.7051	8.7624	0.7051	0.0011
JUL 27 2014	Run59	50um/10Hz	BCR-2G_48	0.00003	0.00000	0.00111	0.03595	0.02050	0.00000	0.02936	0.17969	0.05691	0.7057	8.7659	0.7057	0.0011
JUL 27 2014	Run60	50um/10Hz	BCR-2G_49	0.00004	0.00000	0.00112	0.03534	0.02048	0.00000	0.02909	0.17957	0.05711	0.7052	8.7665	0.7053	0.0011
JUL 27 2014	Run61	50um/10Hz	BCR-2G_50	0.00001	0.00001	0.00118	0.03739	0.02129	0.00000	0.03051	0.18674	0.05794	0.7054	8.7690	0.7055	0.0011
Average and error in 2SD													**0.7052**	**0.0006**	**0.7052**	**0.0006**
AUG 18 2014	Run02	50um/10Hz	BCR-2G_1	0.00003	0.00001	0.00147	0.05007	0.02921	-0.00001	0.04137	0.25609	0.05278	0.7047	8.7684	0.7054	0.0011
AUG 18 2014	Run03	50um/10Hz	BCR-2G_2	0.00005	0.00001	0.00158	0.05033	0.02959	-0.00001	0.04171	0.25925	0.05601	0.7035	8.7603	0.7046	0.0008
AUG 18 2014	Run04	50um/10Hz	BCR-2G_3	0.00005	0.00000	0.00177	0.05833	0.03270	0.00001	0.04718	0.28669	0.05683	0.7031	8.7680	0.7043	0.0011

AUG 18 2014 Run05	50um/10Hz	BCR-2G_4	0.00005	0.00000	0.00171	0.05685	0.03161	0.00000	0.04580	0.27715	0.05679	0.7044	8.7663	0.7046	0.0007
AUG 18 2014 Run06	50um/10Hz	BCR-2G_5	0.00003	0.00001	0.00173	0.05844	0.03230	-0.00001	0.04695	0.28284	0.05606	0.7049	8.7585	0.7049	0.0010
AUG 18 2014 Run08	50um/10Hz	BCR-2G_6	0.00003	0.00001	0.00170	0.05887	0.03265	0.00000	0.04737	0.28590	0.05452	0.7049	8.7569	0.7047	0.0009
AUG 18 2014 Run09	50um/10Hz	BCR-2G_7	0.00003	0.00000	0.00174	0.05903	0.03292	0.00001	0.04762	0.28812	0.05525	0.7050	8.7532	0.7048	0.0007
AUG 18 2014 Run10	50um/10Hz	BCR-2G_8	0.00004	0.00001	0.00173	0.05955	0.03272	0.00000	0.04769	0.28640	0.05529	0.7048	8.7547	0.7046	0.0006
AUG 18 2014 Run11	50um/10Hz	BCR-2G_9	0.00004	0.00002	0.00180	0.06027	0.03293	-0.00001	0.04810	0.28802	0.05727	0.7042	8.7481	0.7042	0.0006
AUG 18 2014 Run12	50um/10Hz	BCR-2G_10	0.00007	0.00002	0.00193	0.06047	0.03322	-0.00001	0.04837	0.29021	0.06082	0.7041	8.7383	0.7050	0.0005
AUG 18 2014 Run14	50um/10Hz	BCR-2G_11	0.00004	0.00001	0.00159	0.05436	0.03018	0.00000	0.04375	0.26427	0.05519	0.7050	8.7563	0.7049	0.0007
AUG 18 2014 Run15	50um/10Hz	BCR-2G_12	0.00005	0.00003	0.00164	0.05442	0.02978	0.00000	0.04347	0.26063	0.05746	0.7048	8.7522	0.7049	0.0007
AUG 18 2014 Run16	50um/10Hz	BCR-2G_13	0.00004	0.00000	0.00167	0.05784	0.03153	0.00000	0.04613	0.27604	0.05530	0.7051	8.7556	0.7049	0.0006
AUG 18 2014 Run17	50um/10Hz	BCR-2G_14	0.00002	0.00000	0.00163	0.05638	0.03072	0.00000	0.04495	0.26905	0.05558	0.7048	8.7570	0.7047	0.0007
AUG 18 2014 Run18	50um/10Hz	BCR-2G_15	0.00002	0.00000	0.00165	0.05704	0.03117	0.00000	0.04556	0.27297	0.05548	0.7054	8.7570	0.7053	0.0006
AUG 18 2014 Run20	50um/10Hz	BCR-2G_16	0.00003	0.00002	0.00169	0.06024	0.03288	0.00001	0.04810	0.28811	0.05375	0.7060	8.7631	0.7057	0.0007
AUG 18 2014 Run21	50um/10Hz	BCR-2G_17	0.00005	0.00001	0.00178	0.06200	0.03338	0.00000	0.04915	0.29231	0.05579	0.7055	8.7576	0.7054	0.0006
AUG 18 2014 Run22	50um/10Hz	BCR-2G_18	0.00004	0.00001	0.00179	0.05980	0.03244	0.00000	0.04758	0.28383	0.05774	0.7057	8.7499	0.7058	0.0006
AUG 18 2014 Run23	50um/10Hz	BCR-2G_19	0.00003	0.00002	0.00172	0.05990	0.03289	0.00000	0.04794	0.28796	0.05477	0.7054	8.7561	0.7051	0.0006
AUG 18 2014 Run24	50um/10Hz	BCR-2G_20	-0.00001	0.00002	0.00151	0.05992	0.03274	-0.00001	0.04788	0.28708	0.04766	0.7063	8.7714	0.7054	0.0005
AUG 18 2014 Run26	50um/10Hz	BCR-2G_21	0.00004	0.00000	0.00181	0.05990	0.03346	0.00000	0.04834	0.29274	0.05646	0.7056	8.7496	0.7055	0.0006
AUG 18 2014 Run27	50um/10Hz	BCR-2G_22	0.00006	0.00002	0.00179	0.05920	0.03300	0.00001	0.04772	0.28875	0.05685	0.7055	8.7502	0.7055	0.0004
AUG 18 2014 Run28	50um/10Hz	BCR-2G_23	0.00004	0.00000	0.00179	0.06155	0.03309	0.00000	0.04874	0.28958	0.05656	0.7054	8.7508	0.7053	0.0006
AUG 18 2014 Run29	50um/10Hz	BCR-2G_24	0.00003	0.00001	0.00140	0.04941	0.02717	0.00000	0.03958	0.23797	0.05406	0.7058	8.7578	0.7055	0.0007
AUG 18 2014 Run30	50um/10Hz	BCR-2G_25	0.00005	0.00000	0.00155	0.05109	0.02840	0.00001	0.04114	0.24857	0.05704	0.7058	8.7528	0.7058	0.0007
AUG 18 2014 Run32	50um/10Hz	BCR-2G_26	0.00002	0.00002	0.00156	0.05429	0.02983	0.00000	0.04347	0.26122	0.05497	0.7053	8.7581	0.7051	0.0008
AUG 18 2014 Run33	50um/10Hz	BCR-2G_27	0.00005	0.00002	0.00149	0.04995	0.02801	-0.00001	0.04039	0.24503	0.05572	0.7054	8.7500	0.7053	0.0007
AUG 18 2014 Run34	50um/10Hz	BCR-2G_28	0.00003	0.00001	0.00147	0.05002	0.02799	-0.00001	0.04041	0.24494	0.05502	0.7054	8.7529	0.7052	0.0006
AUG 18 2014 Run35	50um/10Hz	BCR-2G_29	0.00002	-0.00001	0.00149	0.05062	0.02845	0.00000	0.04098	0.24906	0.05463	0.7050	8.7553	0.7048	0.0007
AUG 18 2014 Run36	50um/10Hz	BCR-2G_30	0.00005	0.00002	0.00157	0.05321	0.02882	0.00000	0.04230	0.25213	0.05713	0.7056	8.7480	0.7056	0.0007
AUG 18 2014 Run38	50um/10Hz	BCR-2G_31	0.00004	0.00000	0.00148	0.05012	0.02778	-0.00001	0.04030	0.24328	0.05586	0.7052	8.7566	0.7051	0.0007
AUG 18 2014 Run39	50um/10Hz	BCR-2G_32	0.00003	0.00000	0.00142	0.04955	0.02739	0.00001	0.03978	0.23976	0.05409	0.7049	8.7556	0.7047	0.0008
AUG 18 2014 Run40	50um/10Hz	BCR-2G_33	0.00004	0.00001	0.00152	0.05214	0.02845	0.00000	0.04159	0.24896	0.05584	0.7051	8.7507	0.7050	0.0006
AUG 18 2014 Run41	50um/10Hz	BCR-2G_34	0.00001	0.00001	0.00137	0.05178	0.02867	0.00000	0.04165	0.25133	0.04997	0.7059	8.7651	0.7052	0.0008
AUG 18 2014 Run42	50um/10Hz	BCR-2G_35	0.00003	0.00002	0.00163	0.05348	0.02997	0.00000	0.04322	0.26214	0.05689	0.7051	8.7485	0.7050	0.0006
AUG 18 2014 Run44	50um/10Hz	BCR-2G_36	0.00003	0.00002	0.00168	0.05801	0.03173	0.00000	0.04635	0.27765	0.05534	0.7057	8.7515	0.7056	0.0007
AUG 18 2014 Run45	50um/10Hz	BCR-2G_37	0.00004	0.00001	0.00162	0.05264	0.02985	-0.00002	0.04278	0.26098	0.05691	0.7049	8.7446	0.7049	0.0005
AUG 18 2014 Run46	50um/10Hz	BCR-2G_38	0.00005	0.00001	0.00160	0.05318	0.02936	0.00002	0.04267	0.25674	0.05683	0.7054	8.7436	0.7054	0.0007
AUG 18 2014 Run47	50um/10Hz	BCR-2G_39	0.00004	0.00001	0.00158	0.05438	0.02924	-0.00001	0.04306	0.25587	0.05664	0.7052	8.7498	0.7052	0.0006
AUG 18 2014 Run48	50um/10Hz	BCR-2G_40	0.00002	0.00003	0.00162	0.05398	0.02945	0.00000	0.04303	0.25764	0.05737	0.7047	8.7474	0.7047	0.0006
AUG 18 2014 Run50	50um/10Hz	BCR-2G_41	0.00003	0.00001	0.00163	0.05523	0.03019	0.00001	0.04409	0.26414	0.05634	0.7053	8.7508	0.7052	0.0005
AUG 18 2014 Run51	50um/10Hz	BCR-2G_42	0.00005	0.00001	0.00169	0.05623	0.03109	0.00000	0.04515	0.27201	0.05679	0.7055	8.7501	0.7055	0.0006
AUG 18 2014 Run52	50um/10Hz	BCR-2G_43	0.00003	0.00002	0.00170	0.05725	0.03141	-0.00001	0.04580	0.27488	0.05648	0.7055	8.7504	0.7055	0.0007
AUG 18 2014 Run53	50um/10Hz	BCR-2G_44	0.00002	0.00001	0.00169	0.05870	0.03214	0.00000	0.04692	0.28136	0.05501	0.7056	8.7540	0.7054	0.0005
AUG 18 2014 Run54	50um/10Hz	BCR-2G_45	0.00004	0.00001	0.00164	0.05592	0.03103	0.00000	0.04498	0.27158	0.05548	0.7055	8.7537	0.7054	0.0005
AUG 18 2014 Run56	50um/10Hz	BCR-2G_46	0.00004	0.00002	0.00159	0.05421	0.03041	-0.00001	0.04385	0.26618	0.05469	0.7055	8.7542	0.7053	0.0006
AUG 18 2014 Run57	50um/10Hz	BCR-2G_47	0.00003	0.00001	0.00169	0.05576	0.03096	0.00001	0.04488	0.27096	0.05726	0.7056	8.7512	0.7056	0.0007
AUG 18 2014 Run58	50um/10Hz	BCR-2G_48	0.00003	0.00001	0.00157	0.05413	0.02990	0.00000	0.04343	0.26160	0.05489	0.7053	8.7505	0.7051	0.0007
AUG 18 2014 Run59	50um/10Hz	BCR-2G_49	0.00002	0.00001	0.00161	0.05519	0.03013	0.00001	0.04404	0.26366	0.05590	0.7052	8.7498	0.7051	0.0010
AUG 18 2014 Run60	50um/10Hz	BCR-2G_50	0.00004	0.00001	0.00180	0.06124	0.03307	0.00000	0.04860	0.28928	0.05701	0.7054	8.7486	0.7054	0.0005
Average and error in 2SD												**0.7052**	**0.0012**	**0.7051**	**0.0008**

Day	Run ID	Crater	Sample	^{83}Kr (V)	$^{83.5}$M (V)	^{84}Sr (V)	^{85}Rb (V)	^{86}Sr (V)	$^{86.5}$M (V)	^{87}Sr (V)	^{88}Sr (V)	^{84}Sr/^{86}Sr	^{87}Sr/^{86}Sr	^{88}Sr/^{86}Sr	^{37}Sr/^{86}Sr cor	2SE
AUG 05 2014	Run09	100um/10Hz	KL2-G	0.00013	0.00001	0.00393	0.01973	0.07168	0.00000	0.05970	0.63032	0.05758	0.70350	8.79421	0.70355	0.00057
AUG 05 2014	Run10	100um/10Hz	KL2-G	0.00012	0.00003	0.00384	0.01932	0.07118	0.00001	0.05917	0.62591	0.05676	0.70355	8.79388	0.70353	0.00047
AUG 05 2014	Run11	100um/10Hz	KL2-G	0.00011	0.00002	0.00367	0.01885	0.06796	0.00001	0.05665	0.59742	0.05673	0.70359	8.79029	0.70356	0.00059
AUG 05 2014	Run12	100um/10Hz	KL2-G	0.00013	0.00001	0.00376	0.01982	0.06933	0.00000	0.05803	0.60958	0.05695	0.70341	8.79209	0.70340	0.00054
AUG 05 2014	Run13	100um/10Hz	KL2-G	0.00012	0.00001	0.00378	0.02076	0.07015	0.00002	0.05902	0.61687	0.05657	0.70357	8.79367	0.70353	0.00063
Average and error in 2SD													**0.70352**	**0.00014**	**0.70351**	**0.00013**
AUG 05 2014	Run15	100um/10Hz	ML3B-G	0.00011	0.00001	0.00293	0.01314	0.05360	0.00000	0.04400	0.47108	0.05741	0.70406	8.78952	0.70410	0.00076
AUG 05 2014	Run17	100um/10Hz	ML3B-G	0.00008	0.00001	0.00245	0.01161	0.04579	0.00001	0.03774	0.40244	0.05632	0.70396	8.78979	0.70389	0.00094
AUG 05 2014	Run18	100um/10Hz	ML3B-G	0.00009	0.00002	0.00249	0.01159	0.04615	-0.00001	0.03801	0.40592	0.05662	0.70403	8.79701	0.70399	0.00086
AUG 05 2014	Run21	50um/10Hz	ML3B-G	0.00012	0.00001	0.00294	0.01308	0.05349	-0.00001	0.04388	0.47018	0.05780	0.70375	8.78968	0.70377	0.00071
AUG 05 2014	Run22	50um/10Hz	ML3B-G	0.00010	0.00001	0.00298	0.01356	0.05483	-0.00001	0.04505	0.48194	0.05702	0.70385	8.78905	0.70380	0.00067
AUG 05 2014	Run23	50um/10Hz	ML3B-G	0.00007	0.00002	0.00311	0.01750	0.05770	-0.00001	0.04867	0.50609	0.05657	0.70382	8.77115	0.70371	0.00070
AUG 05 2014	Run24	50um/10Hz	ML3B-G	0.00007	0.00001	0.00305	0.01683	0.05628	-0.00001	0.04737	0.49375	0.05680	0.70370	8.77283	0.70355	0.00075
AUG 05 2014	Run25	50um/10Hz	ML3B-G	0.00007	0.00002	0.00305	0.01732	0.05636	0.00001	0.04761	0.49432	0.05673	0.70374	8.77143	0.70349	0.00072
Average and error in 2SD													**0.70386**	**0.07973**	**0.70379**	**0.00027**